

DEVELOPMENT OF HIGH PERFORMANCE UNCOOLED INFRARED  
DETECTOR MATERIALS

A THESIS SUBMITTED TO  
THE GRADUATE SCHOOL OF NATURAL AND APPLIED SCIENCES  
OF  
MIDDLE EAST TECHNICAL UNIVERSITY

BY

BAŞAK KEBAPÇI

IN PARTIAL FULFILLMENT OF THE REQUIREMENTS  
FOR  
THE DEGREE OF MASTER OF SCIENCE  
IN  
MICRO AND NANOTECHNOLOGY DEPARTMENT

FEBRUARY 2011

Approval of the thesis:

**DEVELOPMENT OF HIGH PERFORMANCE UNCOOLED INFRARED  
DETECTOR MATERIALS**

submitted by **BAŞAK KEBAPÇI** in partial fulfillment of the requirements for the degree of **Master of Science in Micro and Nanotechnology Department, Middle East Technical University** by,

Prof. Dr. Canan Özgen  
Dean, Graduate School of **Natural and Applied Sciences**

\_\_\_\_\_

Prof. Dr. Mürvet VOLKAN  
Head of Department, **Micro and Nanotechnology**

\_\_\_\_\_

Prof. Dr. Tayfun Akın  
Supervisor, **Electrical and Electronics Eng. Dept., METU**

\_\_\_\_\_

Prof. Dr. Raşit Turan  
Co-supervisor, **Physics Dept., METU**

\_\_\_\_\_

**Examining Committee Members**

Prof. Dr. Raşit Turan  
Physics Dept., METU

\_\_\_\_\_

Prof. Dr. Tayfun Akın  
Electrical and Electronics Eng. Dept., METU

\_\_\_\_\_

Assoc. Prof. Dr. Haluk Kùlah  
Electrical and Electronics Eng. Dept., METU

\_\_\_\_\_

Assist. Prof. Dr. Barış Bayram  
Electrical and Electronics Eng. Dept., METU

\_\_\_\_\_

Dr. Yusuf Tanrıkulu  
MEMS Center, METU

\_\_\_\_\_

**Date:** 14.02.2011

**I hereby declare that all information in this document has been obtained and presented in accordance with academic rules and ethical conduct. I also declare that, as required by these rules and conduct, I have fully cited and referenced all referenced material and results that are not original to this work.**

Name, Surname: Bařak KEBAPÇI

Signature:

# ABSTRACT

## DEVELOPMENT OF HIGH PERFORMANCE UNCOOLED INFRARED DETECTOR MATERIALS

Kebapçı, Başak

M.Sc., Department of Micro and Nanotechnology

Supervisor: Prof. Dr. Tayfun Akın

Co-supervisor: Prof. Dr. Raşit Turan

February 2011, 69 pages

This thesis reports both the optimizations of the vanadium oxide ( $\text{VO}_x$ ) thin film as an active infrared detector material by the magnetron sputtering deposition method and its use during fabrication of proper resistors for the microbolometers. Vanadium oxide is a preferred material for microbolometers, as it provides high TCR value, low noise, and reasonable resistance, and a number of high-tech companies have used this material to obtain state-of-the-art microbolometer arrays. This material is first used in microbolometers by Honeywell, who provides its recipe with license agreements, and there is not much information in the literature for its deposition recipe. This is the first study at METU for development of vanadium oxide thin film for microbolometers.

The  $\text{VO}_x$  material deposition studies started by identifying the deposition parameters of the magnetron sputtering system in order to obtain proper  $\text{VO}_x$  resistors for the readout electronics. The obtained recipe includes high temperature deposition conditions of

$\text{VO}_x$ , however, this causes a diffusion problem on the electrodes, preventing to obtain a good contact to  $\text{VO}_x$ . Also, high oxygen level in the depositions makes a contamination on the electrodes. A number of studies were done to determine a proper electrode material which is proper with the deposition conditions of the  $\text{VO}_x$ .

Characterization of the vanadium oxide samples is done by XRD and XPS measurements to see the relation between the phases and resistivity of the vanadium oxide. It is known that  $\text{V}_2\text{O}_5$  phase provides a high TCR and resistivity value, and the XRD results show that this phase is dominant in the highly-oxygen doped or annealed resistors. The TCR and noise measurements are done using resistors implemented with the developed  $\text{VO}_x$  film, after the etching processes of the both  $\text{VO}_x$  and the electrodes are optimized. The contamination on the electrodes is prevented by the help of a newly designed process. The TCR measurement results show that annealing of the resistors affect the TCR values, i.e., increasing the annealing duration increases the TCR values of the resistors. Two different resistors with different deposition conditions are annealed to see the effect of annealing, where TCR results of the resistors are  $-0.74\%/K$  and  $-0.8\%/K$  before annealing. The TCR values of these resistors increase to  $-1.6\%/K$  and  $-4.35\%/K$ , respectively, after annealing in same conditions, showing that both the deposition conditions and annealing change the TCR significantly. Although good TCR values are obtained, the noise values of the  $\text{VO}_x$  resistors are much higher than the expected values, which suggest a further study to determine the cause of this noise.

Keywords: Microbolometers, vanadium oxide ( $\text{VO}_x$ ), magnetron sputtering method, planar resistors, straight-planar type electrodes, Temperature Coefficient of Resistance (TCR), X-Ray Diffraction (XRD), X-Ray Photoelectron Spectroscopy (XPS).

# ÖZ

Kebabçı, Başak

Yüksek Lisans, Mikro ve Nanoteknoloji Bölümü

Tez Yöneticisi: Prof. Dr. Tayfun Akın

Yardımcı Tez Yöneticisi: Prof. Dr. Raşit Turan

Şubat 2011, 69 sayfa

Bu tez çalışmasında, magnetron sıçratma ile kaplama yöntemi kullanılarak vanadyum oksit filmlerin kızılötesi aktif dedektör malzemesi olarak kullanılabilir şekilde geliştirilmesi ve geliştirilen malzeme kullanılarak mikrobolometre dedektörüne uygun direnç üretimi anlatılmaktadır. Vanadyum oksit, yüksek direnç sıcaklık sabiti, düşük gürültü değeri ve makul direnç değeri ile tercih edilen bir kızılötesi duyarga malzemesidir. Ayrıca dünyanın teknolojisinde önde gelen, bir çok kızılötesi duyarga üreten firmaları da bu malzemeyi kullanmaktadır. Dünyada ilk kez Honeywell şirketi tarafından üretilen vanadyum oksit mikrobolometrelerin bu şirket tarafından patenti alınmıştır ve literatürde Honeywell'in vanadyum oksit kaplama reçetesi hakkında çok fazla bilgi verilmemiştir. Bu çalışmayla, mikrobolometreler için vanadyum oksit malzemesi üretimi ODTÜ'de ilk kez yapılmıştır.

Vanadyum oksit üretimi öncelikle, magnetron sıçratma sistemindeki parametrelerin ODTÜ'de üretilen mikrobolometrelerin okuma devresine uygun olacak şekilde ayarlanmasıyla başlanmıştır. Okuma devrelerine en uygun direnci veren kaplama reçetesi elde edilmiştir. Bu reçeteyle üretilen dirençlerde, vanadyum oksitin çok yüksek kaplanma sıcaklığından dolayı elektrotlarda difüzyon gözlenmiştir. Bu difüzyonu önlemek için de elektrotlarda farklı malzemeler denenmiştir.

Vanadyum oksitin malzeme karakterizasyonu XRD ve XPS yöntemleri kullanılarak yapılmıştır. Bu sonuçlar göstermiştir ki,  $V_2O_5$ , yüksek direnç ve yüksek TCR özelliği gösteren malzeme, tavlama işlemi görmüş veya yüksek oksijenle katkılanmış dirençlerde ortaya çıkmaktadır. Bunun yanı sıra malzemeyle TCR ve gürültü testleri yapabilmek için direnç yapılar oluşturulmuştur, bunun için elektrotların ve vanadyum oksitin oyma işlemlerinin ayarlanması yapılmıştır. Elektrotlardaki difüzyon probleminin getirdiği sorunlardan kurtulmak için yeni bir direnç üretim akışı tasarlanmıştır. TCR sonuçları göstermiştir ki, tavlama, dirençlerin TCR değerlerini artırmaktadır. İki farklı koşulda üretilmiş, düşük dirençli yapılar, tavlandıktan önce sırasıyla:  $-0.74\%/K$ ,  $-0.8\%/K$  TCR değerlerini alırken; tavlandıktan sonra TCR değerleri:  $-1.6\%/K$  and  $-4.35\%/K$  olmuştur. Yüksek TCR değerleri bulunmuş olsa da, malzemenin gürültü değerleri beklenenin çok üstünde çıkmıştır, bu durum malzemenin daha iyi tanınması için, üzerinde daha çok çalışılması gerektiğini göstermektedir.

Anahtar Kelimeler: Mikrobolometre, vanadyum oksit ( $VO_x$ ), magnetron sıçratma ile kaplama yöntemi, düzlemsel dirençler, düz-düzlemsel elektrot tipi, Direnç Sıcaklık Sabiti (TCR), X-Işını Kırınımı (XRD), X-Işını Difraksiyon Spektroskopisi (XPS).

*To the Memory of My Grandmother*

*Sadiye Kebapçı*



# ACKNOWLEDGEMENTS

First and foremost, I would like to present my deepest appreciation and gratitude to my supervisor Prof. Dr. Tayfun Akın for all the opportunities he has provided me during my studies and for his great patience. He always guided me to get out of the problems I have dealt with my graduate life. I feel very lucky to meet him and to have a chance to work with him.

I also would like to thank to my co-supervisor Prof. Dr. Raşit Turan and to Dr. Selim Eminođlu for valuable guidance, supports, and advices through my graduate study.

I would like to thank to Dr. Yusuf Tanrıkulu, for his fellowship, for sharing his knowledge of the subject whenever I need. He encouraged and motivated me and my friends during the graduate study. I also would like to thank to Orhan Akar for his helps and for sharing his experiences with me. His incredible problem solving skill and his unique labor discipline inspired me a lot. I would like to acknowledge Akın Aydemir for his help with the etching trials he carried out and SEM photos he took and for the company.

I would like to thank to my colleagues; Ufuk Şenveli, Alperen Toprak, and Eren Çanga for their contributions on microbolometer research and on my own studies, and also for their friendships. I am grateful to Şeniz Esra Küçük for her help in the testing, and for never-ending friendship. I also would like to thank to Özgecan Dervişođlu for guiding me with her friendly, invaluable advices, and for the helps in the testing, also would like to thank to Selçuk Keskin, and Numan Erođlu for the help in the processes and for their friendship.

Very special thanks to Dr. İlker Ender Ocak, for his encouragement, patience, friendship, and help during my graduate life. He always guided me whenever things tend to go wrong, not only for the problems I met in my graduate life but also in my daily life.

I would like to extend my thanks to Dr. Murat Tepegöz, Dr. Özge Zorlu, and all METU MEMS Research Group: Mert Torunbalcı, Burak Eminođlu, Dinçay Akçören, Uđur

Sönmez, Erdinç Tatar, Serdar Tez, Cavid Musayev, Osman Aydın, Ceren Tüfekçi, Soner Sönmezoğlu, Tunjar Asgarlı, and Alper Küçükkömürler for their never-ending friendships and for making the best possible working environment.

Also, I want to acknowledge the members and staff of METU RF MEMS group, METU BIO-MEMS group, and METU MEMS Research Center facilities for their help and friendship.

Another person I would like to thank to is Sami Eren Önder for his supports during the undergraduate and graduate life. Last but not the least, I would like to thank to my friends, my family; especially my mother Feride Yiğit, for the great support, understanding, encouragement, and incredible patience she showed to me throughout my whole life.

# TABLE OF CONTENTS

ABSTRACT .....	iv
ÖZ .....	vi
ACKNOWLEDGEMENTS .....	ix
TABLE OF CONTENTS .....	xi
LIST OF FIGURES .....	xiv
LIST OF TABLES .....	xviii
1 INTRODUCTION .....	1
1.1 Infrared Radiation and Spectrum.....	2
1.2 Infrared Detection.....	2
1.3 Microbolometers.....	4
1.3.1 Resistive Type Microbolometers.....	5
1.4 Determination of the Active Material.....	7
1.4.1 Vanadium Oxide as an Active Material.....	8
1.5 Magnetron Sputtering Method .....	9
1.6 Research Objectives and Thesis Organization .....	10
2 DEVELOPMENT AND OPTIMIZATION OF VANADIUM OXIDE USING MAGNETRON SPUTTERING METHOD.....	13

2.1	Information about the Sputtering System .....	13
2.2	Processes Done Before the Vanadium Oxide Deposition Trials.....	15
2.2.1	Thickness Uniformity Measurements of the Vanadium Target .....	15
2.2.2	The Electrical Resistivity Test of the Vanadium Target.....	16
2.2.3	Determination of the DC Power and the Pressure.....	17
2.3	Influence of the System Parameters on the Electrical Resistivity of the Vanadium Oxide .....	18
2.3.1	Influence of the Deposition Time.....	19
2.3.2	Influence of the DC Power Applied to the Target.....	20
2.3.3	Influence of the Substrate Deposition Temperature .....	22
2.3.4	Influence of the Annealing Temperature and Annealing Temperature Duration.....	23
2.3.5	Influence of The Argon/Oxygen Flow Rate.....	24
2.4	Conclusion.....	25
3	FABRICATION AND PROCESS OPTIMIZATION OF THE VO <sub>x</sub> RESISTORS	26
3.1	Resistor Type and Mask Selection .....	26
3.2	Fabrication of the Electrodes.....	30
3.2.1	Determination of the Electrode Material .....	30
3.2.1.1	Gold with Adhesion Layers .....	31
3.2.2	Etching Optimization of the Gold Electrodes .....	32
3.2.3	Etching optimization of the Platinum Electrodes.....	36

3.3	Etching Optimization of the VO <sub>x</sub> Resistors .....	38
3.3.1	Not annealed-Low Oxygen Doped Resistors .....	42
3.3.2	Not Annealed-High Oxygen Doped Resistors .....	43
3.3.3	Annealed-Low Oxygen Doped Resistors.....	44
3.3.4	Annealed-High Oxygen Doped Resistors .....	45
3.4	Optimization of the Resistance Values .....	48
3.4.1	Low Resistance Group.....	49
3.4.2	High Resistance Group .....	50
3.5	Conclusion.....	51
4	CHARACTERIZATION AND TEST RESULTS.....	52
4.1	Characterization Results .....	52
4.2	Test Results .....	55
4.2.1	TCR Measurements .....	55
4.2.2	Noise Measurements.....	58
4.3	Conclusions .....	62
	CONCLUSION .....	63
	REFERENCES .....	66
	APPENDIX .....	69

# LIST OF FIGURES

## FIGURES

Figure 1.1: The infrared spectrum and its sub-regions in the whole electromagnetic spectrum [4].	3
Figure 1.2: The spectral exitance with respect to wavelength for different temperatures [5].	4
Figure 1.3: Simplified schematic of a generic microbolometer [9].	5
Figure 1.4: Representative isometric view of a resistive type microbolometer detector.	6
Figure 1.5: The schematic diagram of the DC magnetron sputtering apparatus [9]	9
Figure 2.1: The sputtering system used in vanadium oxide processes in METU MEMS Center.	14
Figure 2.2: The representative figure of a 6” test sample on which the measurement areas are indicated with numbers.	16
Figure 2.3: Four-point probe used in the sheet resistance measurements of the vanadium sputtered sample.	17
Figure 2.4: Resistivity change due to the different DC power values.	21
Figure 2.5: Resistivity change due to the different substrate temperature values.	23
Figure 2.6: Resistivity change due to the different substrate values.	25
Figure 3.1: Representative cross sectional view of a planar resistor.	27
Figure 3.2: Cross sectional view of the (a) sandwich gap-type resistor, (b) the enhanced sandwich type resistor and (c) an enhanced sandwich type resistor with cover layer.	27

Figure 3.3: Cross sectional view of the process steps in the fabrication flow (a) Silicon wafer. (b) Silicon nitride is coated on silicon sample. (c) Electrode layers are coated and patterned. (d) Active material layer is coated on the electrodes. (e) Active material is patterned.....	28
Figure 3.4: (a) Various resistor structures of the 6” resistor mask, (b) a resistor with planar-type electrode.....	29
Figure 3.5: Titanium diffuses into gold, during the depositions at high temperatures...	31
Figure 3.6: Chromium diffuses into gold, during the depositions at high temperatures.	32
Figure 3.7: Various straight-planar electrodes formed by wet etching.....	33
Figure 3.8: Gold walls are occurred on the sides of the openings due to the physical etching of gold in Metal RIE. ....	34
Figure 3.9: The results of the finger electrode etching trials with metal RIE. Fingers are made of 20 nm Cr and 50 nm Au layers, and 0.5 $\mu$ Ti is coated on the photoresist. Etch duration: 50 sec, gas used: Ar and HBr .....	35
Figure 3.10: Pt is not etched by Aqua Regia solution annealed at 100 °C.....	36
Figure 3.11: After 60 seconds etching by metal RIE of the 60 nm thick Pt finger electrodes.....	37
Figure 3.12: A closer look to the resistor sample that is prepared with the recipe of sample 3 given in Chapter 2. ....	39
Figure 3.13 : The resistor samples after etching trials. (a) a structure from the resistor Sample 3 given in Table 3.2, the photoresist is stripped, and (b), structures from the resistor Sample 6 of which the vanadium oxide layer is over etched, the photoresist still remains after etching. ....	42
Figure 3.14: Some of the resistor samples from the sample wafer 9 and 10, respectively. The vanadium oxide layers are totally etched by the developer.....	43

Figure 3.15: Resistors of Sample 14, after etching step of the vanadium oxide layer. ..	44
Figure 3.16: A resistor from the sample 15, inspected after the lithography of the vanadium oxide layer. VO <sub>x</sub> is totally etched by the photoresist developer.....	45
Figure 3.17: (a) To prevent the contamination problem on gold, silicon nitride layer is coated on the gold electrodes first. (b) Then, silicon nitride is opened in the middle of the electrodes. (c) Vanadium Oxide active material layer is deposited after. (d) Silicon nitride is coated on the VO <sub>x</sub> . (e) Then the silicon nitride layer is etched. (f) Vanadium Oxide layer is etched. (g) Last nitride layer is etched.....	46
Figure 3.18: Some of the process steps of the new process flow. (a) after silicon nitride is coated on the electrode layer, (b) after photoresist development of the nitride layer, (the layer in the middle is opened), (c) after the development of the VO <sub>x</sub> layer, which is in the middle of the electrodes. (d) after the etching of the VO <sub>x</sub> , the last step of the new process flow.....	47
Figure 3.19: Resistance measurements are made by the probe station in the clean room. ....	48
Figure 4.1: XRD results of the samples processed in different conditions. In sample 1, the V <sub>2</sub> O <sub>3</sub> phase is dominant. After annealing, in the sample 2, V <sub>2</sub> O <sub>5</sub> phase starts to be dominant. In sample 3, both V <sub>2</sub> O <sub>5</sub> and V <sub>2</sub> O <sub>3</sub> phases are observed.....	53
Figure 4.2: Resistance change with temperature, before annealing of the Sample 2. The TCR of the resistor is calculated as -0.74%/K.....	56
Figure 4.3: Resistance change with temperature, before annealing of the Sample 3. The TCR of the resistor is calculated as 0.8 %/K.....	57
Figure 4.4: Resistance change with temperature, after annealing step of the Sample 2. The TCR of the resistor is calculated as -1.6%/K.....	57
Figure 4.5: Resistance change with temperature, after annealing step of the Sample 3. The TCR of the resistor is calculated as -4.35%/K .....	58



Figure 4.6: Simplified schematic of the noise measurement setup used in the measurements. ....	59
Figure 4.7: The noise measurement result of the 115k resistor. The corner frequency is ~3.28 MHz.....	60
Figure 4.8: The noise measurement result of the 85k resistor. The corner frequency is 2.63MHz.....	61
Figure 4.9: A noise test result of the YBCO resistor, previously measured for the YBCO resistor optimizations [20].....	62

# LIST OF TABLES

## TABLES

Table 1.1: General TCR values for different bolometric materials [11] - [15] .....	7
Table 1.2: Electrical properties of the main phases of the vanadium oxide. ....	8
Table 1.3: Most common companies around the world work on vanadium oxide microbolometers. ....	8
Table 1.4: TCR results of the VO <sub>x</sub> resistors in the literature developed by the magnetron sputtering method. ....	10
Table 2.1: Thickness uniformity results of the 6” vanadium sputtered sample, which show that the uniformity is 2.4 % .....	15
Table 2.2: Dependence of the deposition rate (Å/sec) of the vanadium thin film on the DC power and the chamber pressure. ....	18
Table 2.3: Thickness results due to different deposition times .....	20
Table 2.4: Influence of the DC power on the sheet resistance and the resistivity of VO <sub>x</sub> . ....	21
Table 2.5: Influence of the substrate temperature on the sheet resistance .....	22
Table 2.6: Change of the resistivity due to oxygen/argon flow ratio. ....	24
Table 3.1: Etching trials of the prepared vanadium oxide thin film. ....	40
Table 3.1 (continued): Etching trials of the prepared vanadium oxide thin film. ....	41
Table 3.2: Some of the VO <sub>x</sub> deposition recipes of the “not annealed-low oxygen doped” resistors. ....	42

Table 3.3: Some of the VO<sub>x</sub> deposition recipes of the “not annealed-high oxygen doped” resistors. .... 43

Table 3.4: Some of the VO<sub>x</sub> deposition recipes of the “annealed-low oxygen doped” resistors. .... 44

Table 3.5: Some of the process recipes of the “annealed-high oxygen doped” resistors ..... 45

Table 3.6: The changes of the resistances after different annealing recipes. .... 49

Table 3.7: The resistance measurement results of the some trials. The resistances are over the range of the desired resistance range (50-100 kΩ) ..... 50

Table 4.1: Different recipes applied to VO<sub>x</sub> samples for XRD measurements. .... 52

Table 4.2: Comparison of the core level binding energies of the samples. .... 54

Table 4.3: Resistance and TCR variations of the resistors before and after annealing step. .... 55

Table 4.4: The recipes of the samples which are prepared for the noise measurements. 60

# CHAPTER 1

## INTRODUCTION

The curiosity of the mankind to see in dark generated the idea of the “infrared detectors.” Basic mechanism of the infrared detectors relies on the principle that every object that has a temperature above 0 K emits infrared radiation, and the information taken from the objects can be used to see the target. Infrared detectors transform the information coming from the target to an imaging data.

There are two major categories for the infrared detectors: Photon detectors and thermal detectors. The fields of application for these two types are not the same, i.e., thermal detectors are not actually substitutes for photon detectors and vice versa. However, portability and low prices make the thermal detectors more attractive. The working mechanism of the thermal detectors is based on the thermally sensitive structures. Some of these thermally sensitive structures need a specific material that changes its physical properties after collecting the emanation coming from the target. This specific material is called the “active material.”

In the development of the infrared detectors, active materials take a large part, since they identify the sensitivity of the detectors. Therefore, the material must be developed and characterized to increase the performance of the detectors. This thesis reports the development of an active material, namely, vanadium oxide, used for the resistive microbolometers. The resistance of this material changes by the change of the temperature.

The rest of this chapter gives more information about the infrared radiation and detection. Section 1.1 gives information about the infrared radiation and infrared spectrum, and Section 1.2 explains the infrared detection. Section 1.3 and Section 1.4 give information about the microbolometers and determination of the active material, respectively. Section 1.5 explains the operation of the magnetron sputtering system

used for depositing the active material. Finally, Section 1.6 summarizes the objectives of this research and the organization of this thesis.

## 1.1 Infrared Radiation and Spectrum

The nature of the infrared radiation was unknown till 1800. William Herschel, an astronomer working in Bath, was interested in the radiation received from the Sun. He used telescopes in his researches to see the light coming from the Sun and used dark glass filters to reduce its intensity. His measurements with different filters showed that the transmittance of the heat and the light were varying each time he repeated the experiments [1]. This observation led him to demonstrate the existence of radiation beyond the red end of the visible light.

Interaction of radiation with matter is the study of electromagnetic spectroscopy. Our eyes can detect very limited range of this spectrum, the range is between 300 and 800 nm, whereas infrared spectrum spans a section between 0.75 and 1000  $\mu\text{m}$  [2]. Figure 1.1 shows the infrared spectrum and its sub-regions. Different absorption values of the molecules in the air make different atmospheric transmission regions [3]. As can be seen from this figure, there are maximum and minimum regions which identify the operating ranges of the infrared detectors.

## 1.2 Infrared Detection

Every object absorbs electromagnetic radiation to some degree. An object that absorbs all radiation falling on it, at all wavelengths, is called “black body.” For a blackbody object, the spectral exitance is given as:

$$M(\lambda, T) = \frac{2\pi hc^2}{\lambda^5 (e^{hc/\lambda kT} - 1)} \quad (1.1)$$

where  $M(\lambda, T)$  is the spectral exitance,  $h$  is the Planck’s constant,  $c$  is the speed of the light,  $\lambda$  is the wavelength, and  $T$  is the temperature of the object. This equation tells that, when temperature increases, the spectral exitance which means the radiation level that an object emits also increases. In this equation, the  $\lambda$  factor in the denominator is quite effective to change the spectral exitance.

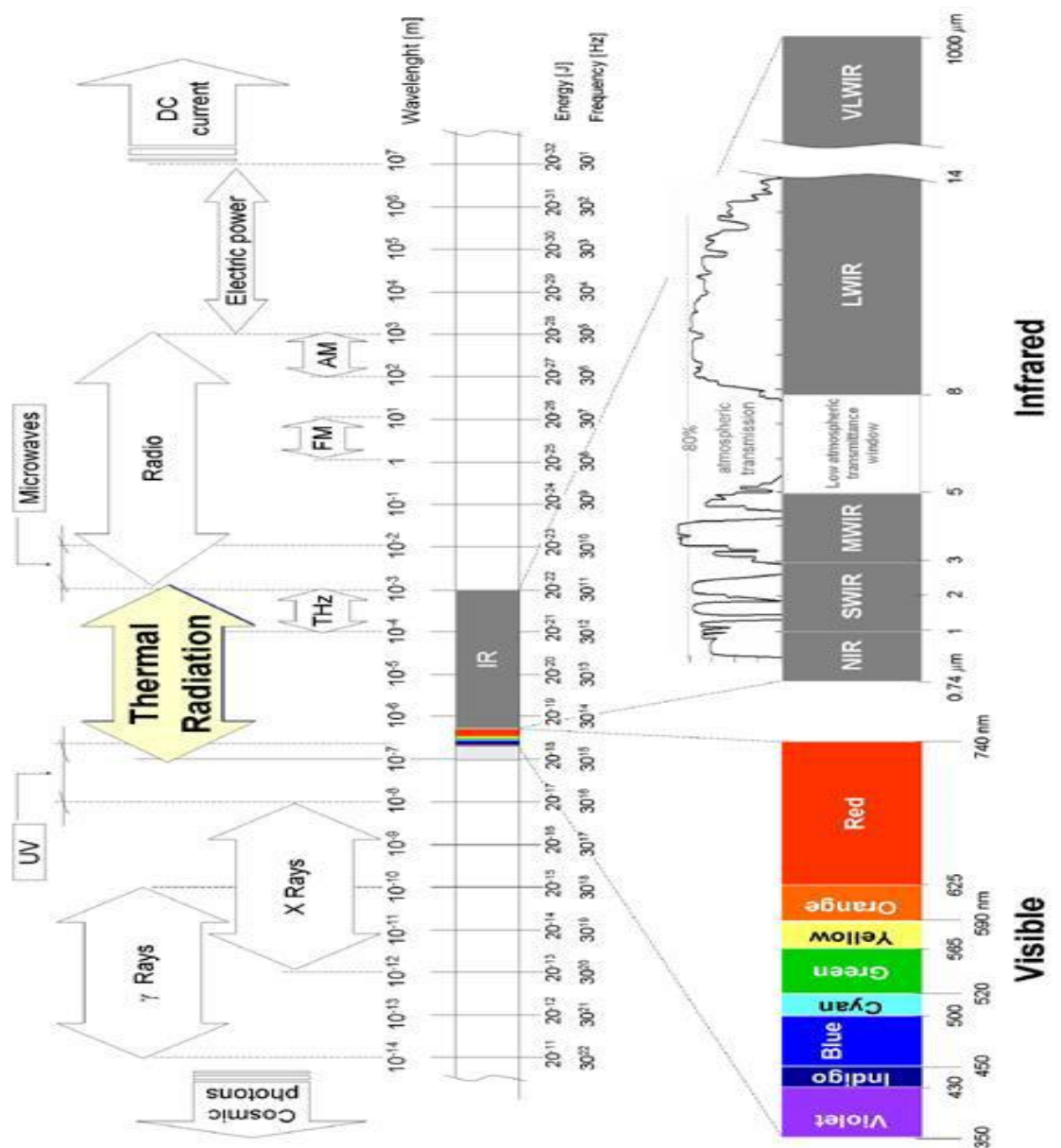


Figure 1.1: The infrared spectrum and its sub-regions in the whole electromagnetic spectrum [4].

Figure 1.2 shows the role of the wavelength on spectral exitance; as the temperature increases the maximum exitance occurs at smaller wavelengths [5]. The straight line given in Figure 1.2 shows the wavelength of the maximum exitance at different temperatures. Maximum exitance value is critical for the infrared detectors and this

value is 10  $\mu\text{m}$  for room temperature  $\sim 300\text{ K}$ . This value can be calculated from the Wien's Displacement Law:

$$\lambda_{max} = \frac{2898}{T} \quad (1.2)$$

where  $\lambda_{max}$  is the wavelength of maximum exitance in  $\mu\text{m}$  and  $T$  is the temperature of the object in K. From Equation 1.2, it can be easily seen that the most convenient region is the 8-12  $\mu\text{m}$  bandwidth for targets in room temperature, whereas for hotter objects, the 3-5  $\mu\text{m}$  bandwidth is better.

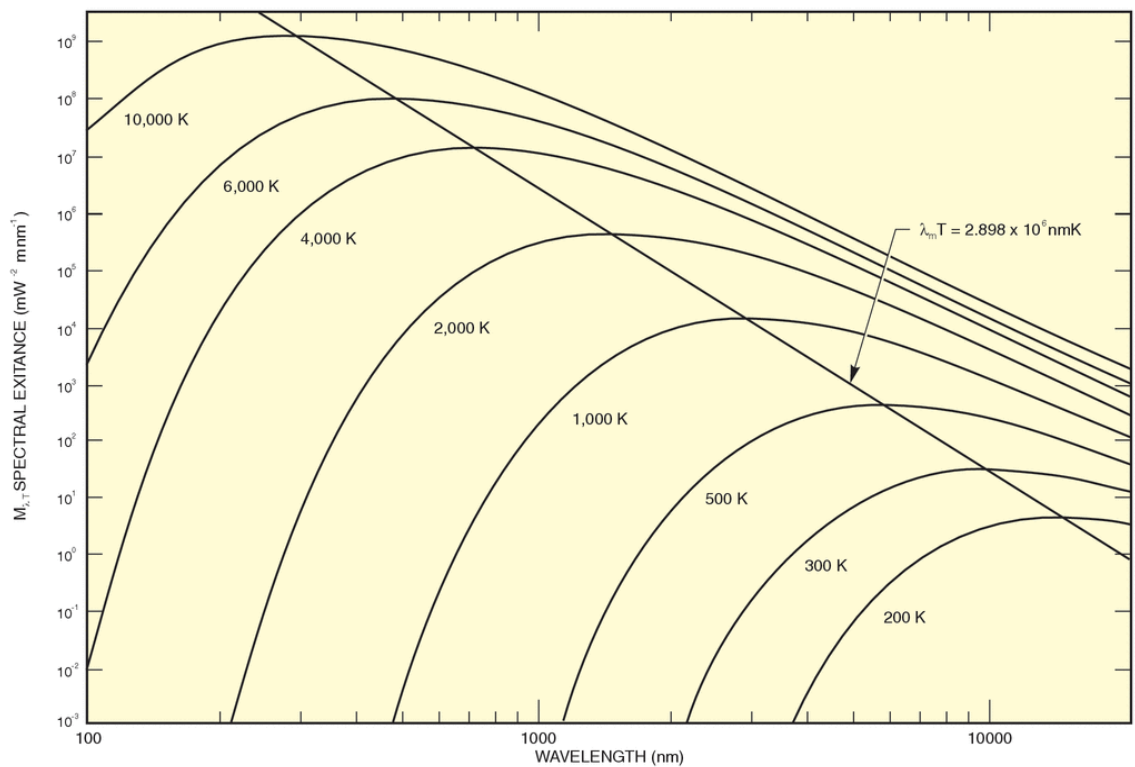


Figure 1.2: The spectral exitance with respect to the wavelength for different temperatures [5].

### 1.3 Microbolometers

Microbolometers are one type of the uncooled infrared detectors. They are produced by simple micro-fabrication process. Advanced silicon CMOS technology has positioned

microbolometer imaging systems for a wide range of thermal imaging applications, such as weapon and vehicle sights, security, defense, medical examination, fire fighting, and industrial detection, which all require compact, cheap, and room-temperature infrared cameras [6].

The operating principle of the microbolometers is based on measuring the physical property change on the active temperature sensitive materials. Figure 1.3 shows a generic microbolometer.

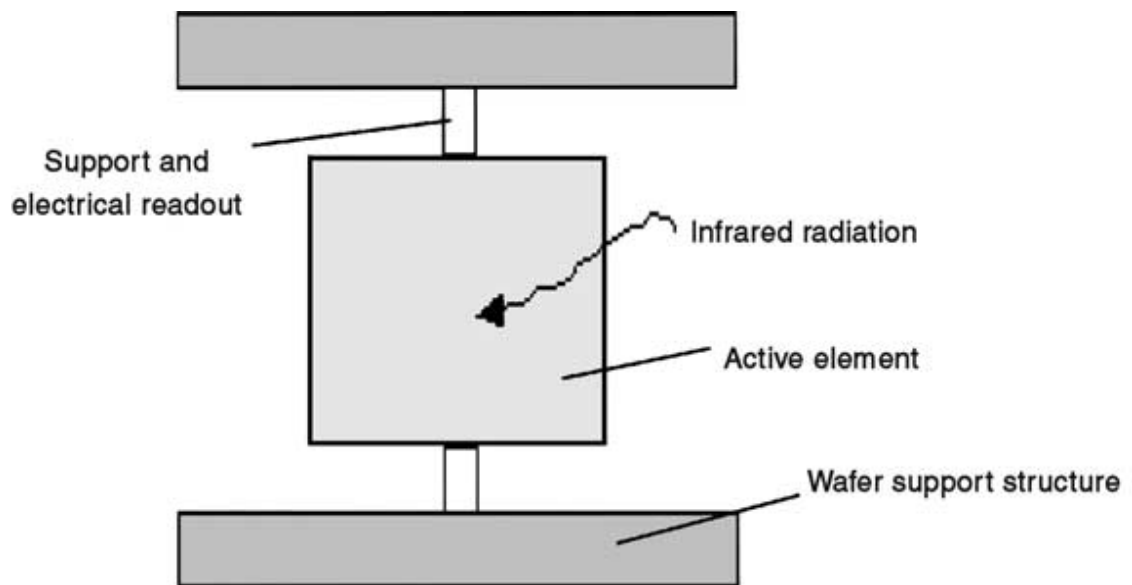


Figure 1.3: Simplified schematic of a generic microbolometer [7].

Microbolometers can be classified under two types according to their temperature sensing architectures. Resistive type microbolometers are one type of the microbolometers, where the second one is the diode type microbolometers. Several other thesis [6], [8], [9] can be referenced for further information on uncooled microbolometer detectors.

### 1.3.1 Resistive Type Microbolometers

In resistive type microbolometers, the physical property that changes with the infrared radiation is resistance. Figure 1.4 shows a representative figure of a resistive type microbolometer. When the infrared radiation is absorbed, there occurs a temperature increase that causes a change in the temperature sensitive material that is located in the



middle of the microbolometer pixel. Then, this change is measured by the aid of a monolithically integrated CMOS circuitry [6]. Temperature coefficient of resistance (TCR) of the active material is an important parameter to determine the amount of this change.

TCR demonstrates how rapidly the electrical resistance change responds to the change of the temperature, and it is used to quantify the sensitivity of the detector. It can be positive or negative depending on the material used in the detector. TCR “ $\alpha$ ” is found from the following equation.

$$\alpha = \frac{1}{R} \frac{dR}{dT} \quad (1.3)$$

where  $R$  is the total resistance of the detector and  $T$  is the temperature.

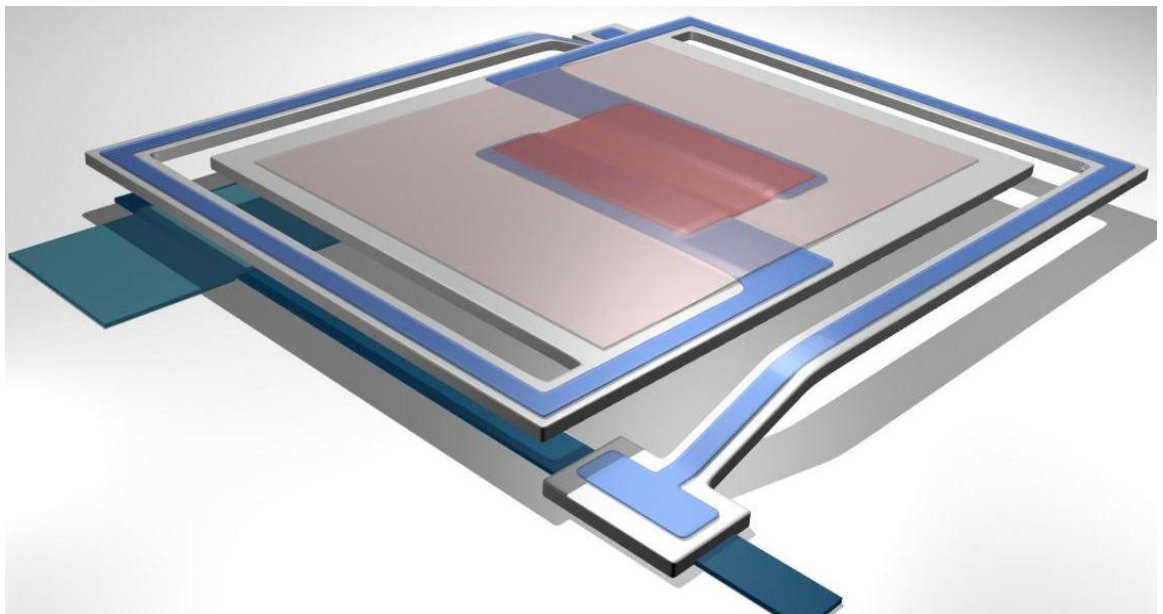


Figure 1.4: Representative isometric view of a resistive type microbolometer [6].

Active material characterization has a dominant role in the resistive type microbolometers. The sensitivity of the active material also determines the sensitivity of the detector. Thus, thermal sensitive materials having high TCR values are essential for all of the infrared detectors.

## 1.4 Determination of the Active Material

Determining the active material is the most important thing for the resistive type microbolometers. Resistance value, TCR, and the noise values of the active material determine the performance of the detectors. The resistivity of the active material should not be very high, since the high resistivity causes high 1/f noise [10]. Also, TCR value of the material is very critical, since the TCR of the material should be as high as possible. However, while trying to increase the TCR value; undesired changes on the noise and the resistivity of the material should be prevented, and the process conditions should be optimized considering all of these parameters together.

The most common active materials for microbolometers are vanadium oxide ( $\text{VO}_x$ ), amorphous silicon (a-Si), Poly-Si, YBCO, polycrystalline SiGe (poly-SiGe), and  $\text{La}_x\text{Ca}_{1-x}\text{MnO}_3$ . Table 1.1 shows the typical TCR values given in the literature for these active materials. Vanadium oxide has the lowest noise value when the noises of the active materials given in Table 1.1 are compared [11].

Table 1.1: General TCR values for different bolometric materials [11].

MATERIAL	TCR (%/K)	Required Process Temperature (°C)
$\text{VO}_x$	-2	~300
a-Si:H	-2.5 to -4	<400
SiGe (30%)	- 2.5	< 650
YBCO	-3 to 3.5	~25
$\text{La}_x\text{Ca}_{1-x}\text{MnO}_3$	10-30	~800
Poly-Si	-0.7 to -3.7	~600

As it is seen from the table, when the working temperature limit of the CMOS circuits (~400 °C) is considered, the most proper active materials for the detectors are  $\text{VO}_x$  and YBCO. Until the study performed in the framework of this thesis, YBCO has been used as an active material in the resistive type microbolometers developed in METU MEMS Research Group. As a resistor material, YBCO is similar to  $\text{VO}_x$ . They are both semiconductors, and their resistivity increase when they absorb oxygen from air. In addition to this, it is observed that in both of the materials, annealing has a great

influence on the resistivity of the films. Their resistivity values increase by increasing the annealing durations [7].

#### 1.4.1 Vanadium Oxide as an Active Material

$VO_x$  has a mixed form material.  $VO_2$ ,  $V_2O_3$ , and  $V_2O_5$  are the main phases seen in the  $VO_x$ .  $VO_2$  and  $V_2O_5$  are very resistive structures, and also their TCR values are higher than the TCR of  $V_2O_3$  [7].  $V_2O_3$  is found very often in  $VO_x$ , because its phase transition is at very low temperatures like 139 K [12]. Table 1.2 shows the electrical properties of the main phases of the vanadium oxide.

Table 1.2: Electrical properties of the main phases of the vanadium oxide.

PHASE	PROPERTIES
$V_2O_5$	High Resistivity-High TCR
$VO_2$	Lower Resistivity-High TCR-Difficult to achieve
$V_2O_3$	Low Resistivity-Low TCR

$VO_x$  has been used as an ideal thermal sensitive material of far infrared 8–12  $\mu\text{m}$  uncooled focal plane arrays, because of its high TCR and low noise values [11]. Among the state of the art microbolometers, TCR of the vanadium oxide changes between -1%/K and -3%/K at 300 K and they have relatively low 1/f noise and a high IR absorption [11]. Table 1.3 shows the most common companies work on the  $VO_x$  microbolometers.

Table 1.3: Most common companies around the world work on vanadium oxide microbolometers.

Country	USA						France	Japan		Israel
Company	Honeywell	FLIR	BAE	DRS	Raytheon	L-3	ULIS	Mitsubishi	NEC	SCD

## 1.5 Magnetron Sputtering Method

There are a number of deposition methods that have been utilized to deposit  $\text{VO}_x$  thin films, including sputtering [13], evaporation, chemical vapor deposition, pulsed laser deposition, as well as sol-gel methods. In this thesis, magnetron sputtering technique is used to develop the  $\text{VO}_x$  active material [14].

In magnetron sputtering method, it is possible to deposit almost all kinds of materials by modifying various parameters in the system. These system parameters are discussed in detail in Chapter 2. Figure 1.5 shows the schematic diagram of the DC magnetron sputtering apparatus.

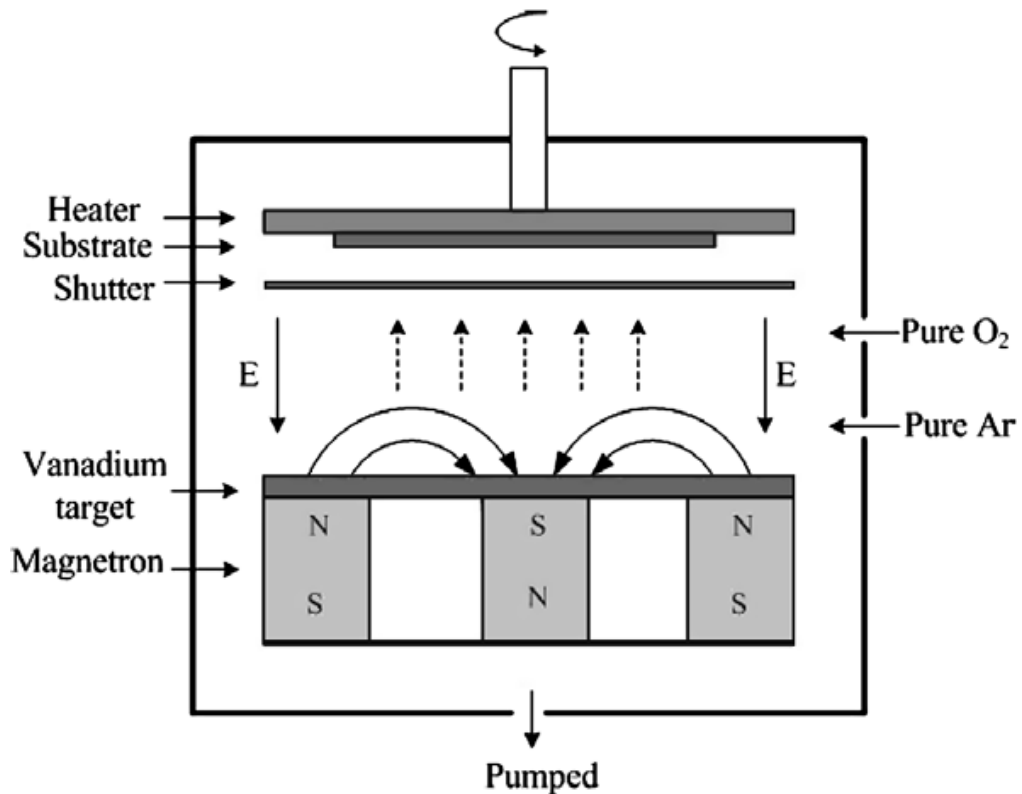


Figure 1.5: The schematic diagram of the DC magnetron sputtering apparatus [7].

A high magnetic field is generated by the use of magnetrons. Secondary electrons generated during the sputtering process are trapped in this field and stay close to the cathode surface. Following helical paths around the magnetic field lines, these electrons are forced to travel longer distances inside the chamber, and thus induce more ionizations, and finally increase the sputter yield,  $S$ , with a significant amount.

The sputter yield  $S$  can be calculated using the following equation:

$$S = \frac{\text{atoms removed}}{\text{incident ions}} \quad (1.4)$$

Sputter yield mostly depends on the incident ion's energy, target material, incidence angle, and target structure.

There are many groups that use the magnetron sputtering technique in their  $\text{VO}_x$  microbolometer or resistor studies. Table 1.4 shows some of these studies and the TCR results of the  $\text{VO}_x$  resistors.

Table 1.4: TCR results of the  $\text{VO}_x$  resistors in the literature developed by the magnetron sputtering method.

Studies	TCR Values
S. Chen et al.-2007 [14]	-1.9%/K
J. Dai et al. -2007 [7]	-2.05%/K
S. Chen et al.-2005 [13]	-2.0%/K

The main parameters that should be controlled in the magnetron sputtering system are DC power, chamber pressure, substrate temperature, tilt of the target, and the distance between the target and the substrate. The details of these optimizations are shown in Chapter 2.

## 1.6 Research Objectives and Thesis Organization

The aim of this research is to develop and optimize CMOS compatible  $\text{VO}_x$  thin film material by using the magnetron sputtering method in order to get high TCR value, optimum resistance, and low  $1/f$  noise values for resistive microbolometers.  $\text{VO}_x$  resistors are fabricated and optimized to measure the performance parameters of the material. The specific objectives are listed below:

1. *Optimization of the deposition conditions by using the magnetron sputtering method.* All the deposition parameters used in the sputtering system affect the characteristic of the  $\text{VO}_x$  films. Therefore, the optimization of the parameters should be done by

considering the change observed in the resistivity and the thickness of the vanadium oxide. Thus, it can give an idea in the resistor fabrication, about which process recipe should be used to achieve a proper resistance value.

*2. Selection of the proper resistor and electrode type for the resistivity of the deposited vanadium oxide.* The resistance values of the resistors are significant. In the microbolometers developed in METU, the proper resistance values are changing between 50-100 k $\Omega$ . To achieve these values, the resistivity of the vanadium oxide should be determined first. Since the resistivity of the vanadium oxide, which is used as a high performance active material, changes over a large range, the identification of the resistor or electrode type is critical for the VO<sub>x</sub> resistors.

*3. Optimization of the wet and dry etching of the electrodes of the VO<sub>x</sub> resistors, and also optimization of the vanadium oxide etching.* These processes are both necessary and critical to be able to fabricate a VO<sub>x</sub> resistor, on a suspended pixel structure.

*4. Investigation of the material with X-Ray Diffraction and XPS to make a relation between the material characteristic and the TCR, noise, resistance values of the resistors.* Since the VO<sub>x</sub> is a fixed phase material, the phases observed will be quite helpful to understand the influences of the phases on the resistance, TCR, or noise of the VO<sub>x</sub>. All these studies also give an overall idea about the relation between the deposition conditions and material characteristic.

The rest of this thesis is organized as follows:

Chapter 2 gives information about the optimization of the vanadium oxide sputtering by the magnetron sputtering system. It identifies the influence of the system parameters on the deposition of the VO<sub>x</sub>, gives the sheet resistance and the thickness measurement results of the vanadium oxide thin films.

Chapter 3 tells the fabrication of the vanadium oxide resistors with optimum resistance values. It identifies the problems encountered during the fabrication process, gives some solutions to these problems, and categorizes the deposition of the VO<sub>x</sub> due to these problems.

Chapter 4 gives the characterization measurements of the VO<sub>x</sub> thin films, including their TCR and noise. It gives the relation between the expected values and the measured values in detail.

Chapter 5 gives conclusion of this thesis work and mentions the future works related to this study.

## CHAPTER 2

# DEVELOPMENT AND OPTIMIZATION OF VANADIUM OXIDE USING MAGNETRON SPUTTERING METHOD

This chapter presents the development of vanadium oxide ( $\text{VO}_x$ ) by the magnetron sputtering method. It gives the parameters that should be optimized to be able to utilize this semiconductor compound as an active detector material and the results of the experiments depending on these parameters. Section 2.1 gives the information about the sputtering system, and Section 2.2 describes the processes done before starting the optimizations. Section 2.3 defines the deposition parameters, namely, the deposition time, the applied DC power, the deposition temperature, the annealing temperature-annealing duration, and the oxygen/argon ratio. It also presents the influences of these parameters on the sheet resistance, thickness, and electrical resistivity values of the vanadium oxide thin film. Section 2.4 summarizes all the parameters mentioned in Section 2.3 and gives an overall idea about the relation between the magnetron sputtering system parameters and the electrical resistivity of the fabricated vanadium oxide film.

### 2.1 Information about the Sputtering System

As previously mentioned, this thesis introduces the fabrication of vanadium oxide by a sputtering system, working principle of which is based on the magnetron sputtering technique.

In the sputtering system used in METU MEMS Center (namely, AJA Sputtering System), there are two gas inlets. Oxygen and argon gases are introduced into the chamber through these inlets by the aid of the valves. Inside the chamber, there is a rotating deposition system. Since the substrate is rotating during the deposition, the uniformity of the depositions is better than the non-rotating systems.



A vanadium target is used to obtain vanadium oxide films. During the deposition, while the vanadium sputtering is taking place, oxygen gas enters the system and oxidizes the vanadium coated sample, which is called as reactive sputtering. Figure 2.1 shows a picture of the sputtering chamber with the vanadium target. There are different biasing options to sputter the vanadium target [15]. Among them, DC and RF biasing are used in the sputtering systems in the clean room facilities. For vanadium oxide deposition, DC biasing is more preferable than RF biasing, since the target is a metal [16]. It is also claimed that structural and electrochemical properties of  $VO_x$  is better when DC reactive sputtering is chosen [17]. Therefore, vanadium target is biased with DC bias voltage during the optimizations.



Figure 2.1: The sputtering system used in the vanadium oxide depositions in METU MEMS Center.

## 2.2 Processes Done Before the Vanadium Oxide Deposition Trials

Before starting to optimize the vanadium oxide depositions, some processes should be done such as the resistivity check of the vanadium target, thickness measurements throughout a 6” coated wafer to see the thickness uniformity of the vanadium oxide film, and determination of the DC Power and the chamber pressure.

### 2.2.1 Thickness Uniformity Measurements of the Vanadium Target

The thickness uniformity has an important role on the microbolometer process. In the thickness uniformity tests, the power and chamber pressure values are chosen to be the same as the ones set for the resistivity measurements. Figure 2.2 shows the representative figure of a 6” test sample on which the measurement areas are indicated with numbers. Table 2.1 lists the results of the thickness uniformity measurements throughout the wafer. Thickness measurements of the wafer prepared for electrical resistivity test was done with a film thickness measuring profilometer (Veeco Dektak 8). The process recipe of the sample is as follows:

- Argon Flow: 26 sccm
- Chamber Pressure: 6 mTorr
- DC Power: 350 W
- Temperature: 300 K

Table 2.1: Thickness uniformity results of the 6” vanadium sputtered sample, which show that the uniformity is 2.4 %.

Position	Thickness	Position	Thickness
1	141nm	6	145nm
2	144nm	7	144nm
3	140nm	8	147nm
4	145nm	9	146nm
5	140nm		

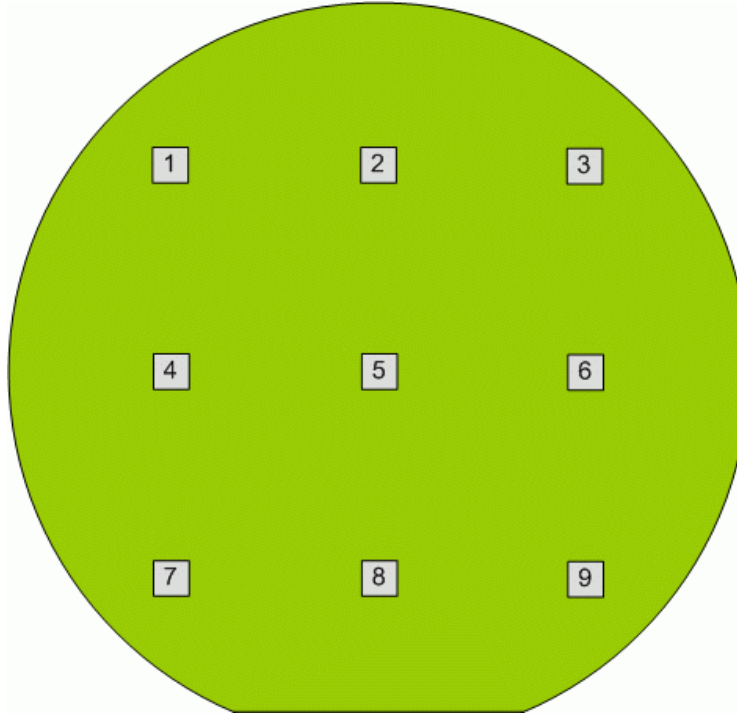


Figure 2.2: The representative figure of a 6” test sample on which the measurement areas are indicated with numbers.

Using the data given in Table 2.1 and Equation 2.1 given below, calculated average non-uniformity value is found as 2.4%.

$$\text{non uniformity} = \frac{\text{max. measured value} - \text{min. measured value}}{2 \times \text{average}} \times 100 \quad (2.1)$$

The value found for the thickness non-uniformity is sufficient for the vanadium oxide optimization processes. The tilt of the substrate and the distance between the target and the substrate is fixed as 20° and 30 mm, respectively.

### **2.2.2 The Electrical Resistivity Test of the Vanadium Target**

The electrical resistivity of the vanadium target should be comparable with the resistivity values given in the literature. In order to see it, sheet resistance measurements of the sample prepared for the thickness non-uniformity measurement is

done. Figure 2.3 shows the four-point probe used in the sheet resistance measurements of the vanadium sputtered sample.

The average sheet resistance values measured throughout the wafer is  $1.25 \Omega/\square$ . The average resistivity is calculated using Equation 2.2 as  $\sim 180 \text{ n}\Omega\cdot\text{m}$ , and this resistivity value is acceptable because it is given as  $197 \text{ n}\Omega\cdot\text{m}$  at  $20 \text{ }^\circ\text{C}$  in the literature [18].

$$\rho = R_s \times d \quad (2.2)$$

where  $\rho$  is the resistivity of the material,  $R_s$  is the sheet resistance, and  $d$  is the thickness of the material.



Figure 2.3: Four-point probe used in the sheet resistance measurements of the vanadium sputtered sample.

### 2.2.3 Determination of the DC Power and the Pressure

Process parameters are adjusted by changing them systematically and thickness is read over the thickness monitor. The electrical property of the vanadium is saved into the system settings. Table 2.2 shows the dependence of the deposition rate on the DC power and the chamber pressure. During this sputtering process following recipe is used:

- Argon flow: 45 sccm
- Temperature: 300K
- No annealing.

Table 2.2: Dependence of the deposition rate ( $\text{\AA}/\text{sec}$ ) of the vanadium thin film on the DC power and the chamber pressure.

Power		100W	150W	200W	250W	300W	350W	400W	450W
Pressure (mTorr)	1	0.2	0.3	0.4	0.5	0.6	0.7	0.9	1.0
	2	0.1	0.2	0.3	0.4	0.5	0.6	0.7	0.8
	5	0.1	0.2	0.3	0.3	0.4	0.5	0.6	0.7
	10	0.1	0.1	0.2	0.3	0.3	0.4	0.5	0.6

The maximum chamber pressure and the maximum power are set to 10 mTorr and 450 W, respectively. In Table 2.2, it is evident that maximum power and minimum pressure maintains the maximum deposition rate. However, in the literature, during the depositions of  $\text{VO}_x$  with the magnetron sputtering, chamber pressure is set to  $\sim 7$  mTorr [7, 13, 14]. By considering this, the deposition pressure is fixed to 7 mTorr, and the applied power is determined as 450 W at first in order to get higher deposition rates.

### 2.3 Influence of the System Parameters on the Electrical Resistivity of the Vanadium Oxide

There are various parameters to be optimized in a magnetron sputtering system for each different material deposited. These parameters are as follows: the deposition time, the power applied to the target, the deposition temperature, the annealing temperature, and the oxygen/argon ratio or oxygen partial pressure inside the chamber. The experiments show that the oxygen ratio in the chamber and the temperature of the substrate during deposition are the most effective ones on the resistivity or sheet resistance values of the thin film vanadium oxide. Especially the oxygen ratio and the temperature of the substrate should be well optimized to transform the “vanadium” metal into the “vanadium oxide” semiconductor material that is used as an active layer for microbolometers.

### 2.3.1 Influence of the Deposition Time

The deposition time is an important factor in the sputtering system, as it determines the thickness of the coated material. The thickness of the active material layer should be in a range that can be etched easily. In the literature, the thickness of the vanadium oxide thin film used in the microbolometers changes between 30 nm-300 nm. When the thickness increases, the sheet resistance value of the  $\text{VO}_x$  thin film decreases, as expected.

The experiments with vanadium oxide showed that up to thicknesses of ~150 nm by increasing thickness, the sheet resistance decreases and the resistivity value does not change as expected. However, after the 150-200 nm thicknesses, the sheet resistance value also starts to increase. There is a similar study in the literature that confirms this fact [19]. According to this study, increasing the film thickness increases the resistivity since the material transforms into the  $\text{V}_2\text{O}_5$  phase which is a very resistive one. This reference also indicates that thicker vanadium oxide films precisely exhibit  $\text{V}_2\text{O}_5$  structures in its form.

There is another factor that should be considered in the thickness optimizations. This factor is the optimum resistance value for the detector readout in the resistive type microbolometers. The range within which the resistors are fabricated should be compatible with the readout circuit. This range is 50-100 k $\Omega$  in the microbolometer readout circuits designed at METU, as the readout electronics are optimized for these values, which are determined considering the typical resistance values obtained with YBCO resistors. The thickness optimization is carried out while considering this resistance range. However, the thickness is related not only with the deposition time, but also with the Ar /O<sub>2</sub> ratio in the chamber.

The experiments show that during the deposition, when the O<sub>2</sub> ratio increases, the deposition rate decreases, which in turn decreases the thickness. This property of the sputtering should be considered while estimating the deposition time of the process. Table 2.3 shows the deposition time and the corresponding average thickness values. The recipe used for the measurements given in this table is same for all three samples and the recipe parameters are chosen as follows:

- Ar:O<sub>2</sub> : 45:3 (sccm)
- Pressure: ~6 mTorr
- DC power: 450 W
- Temperature: 300K
- no annealing

Table 2.3: Thickness results due to different deposition times.

Deposition Time	Measured Thickness
500 sec	62 nm
1000 sec	120 nm
1500 sec	170 nm

Deposition time is set to 1000 seconds which is proper for the high or low oxygen contents.

### 2.3.2 Influence of the DC Power Applied to the Target

When the other parameters are kept constant, it is observed that different power values cause different resistivity values. Four different DC power levels (200 W, 300 W, 350W, and 450 W) are applied to the target and the changes of the resistivity values are observed. Table 2.4 gives the applied DC power values and the corresponding sheet resistance and thickness values. It shows that the resistivity increases while decreasing the DC power. The resistivity corresponding to 200 W could not be read by the four point probe, since the resistivity value was over its working range. Therefore, another four-point probe measurement system (namely, Quad Pro) is used in those trials.

The recipe used for the measurements given in Table 2.4 as follows:

- Ar:O<sub>2</sub> : 15:3 (sccm)
- Deposition Time: 1000 sec.
- Pressure: ~5.6 mTorr
- Temperature: 25°C, and no annealing.

Table 2.4: Influence of the DC power on the sheet resistance and the resistivity of VO<sub>x</sub>.

Sample Number	DC Power (W)	Avg. Sheet Resistance ( $\Omega/\square$ )	Avg. Thickness (nm)	Avg. Resistivity ( $\Omega\cdot\text{cm}$ )
1	200	$\sim 5.7 \times 10^9$ (measured with Quad Pro)	$\sim 112$	$\sim 63.8$ k
2	300	$\sim 3.5 \times 10^7$	$\sim 117$	$\sim 409.5$
3	350	$\sim 0.2 \times 10^7$	$\sim 128$	$\sim 25.6$
4	450	$\sim 0.4 \times 10^6$	$\sim 125$	$\sim 5$

Figure 2.4 shows the graph that identifies the resistivity change due to the DC power of the system. It is clear that the DC power applied to the sputtering target has a major effect on the resistivity of the vanadium oxide thin film. The thickness values of the thin film also changes excessively. The resistivity or sheet resistance of the material can be controlled using this process parameter.

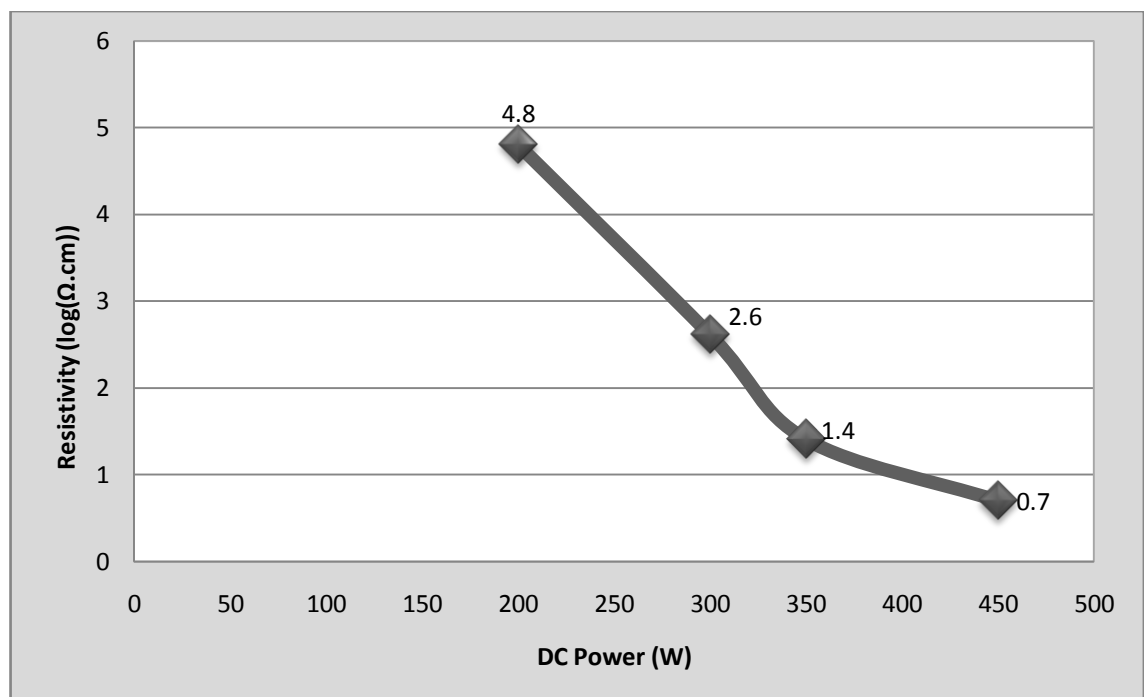


Figure 2.4: Resistivity (logarithmic) change due to the different DC power values.



### 2.3.3 Influence of the Substrate Deposition Temperature

The deposition temperature influences the resistivity of the material as the deposition time and the applied power. In the literature, most research groups claim that increase of the deposition temperature increases the TCR of vanadium oxide films [13, 14]. Also, most of these studies are in the temperature range of 200-300°C.

In order to see the influence of the substrate temperature, the substrate is heated to different deposition temperatures as 200 °C, 250 °C, and 300 °C while the other parameters are kept constant. Table 2.5 shows the sheet resistance and the thickness values corresponding to each substrate temperature.

The recipe used for the measurements given in Table 2.5 as follows:

- Ar:O<sub>2</sub> flow : 15:3 sccm
- Deposition time: 1000 sec
- Pressure: ~5.6 mTorr
- DC power: 350 W
- No Annealing.

Table 2.5: Influence of the substrate temperature on the sheet resistance

Sample Number	Substrate Temperature	Avg. Sheet Resistance ( $\Omega/\square$ )	Avg. Thickness (nm)	Avg. Resistivity ( $\Omega.cm$ )
3	300 °C	$0.2 \times 10^7$	128	25.6
5	250 °C	$0.8 \times 10^6$	128	10.2
6	200 °C	$0.35 \times 10^6$	129	4.5

300 °C is set as an upper temperature limit to comply with the temperature limitations in the post-processing of CMOS substrates. Figure 2.5 shows the resistivity change due to temperature change of the substrate.

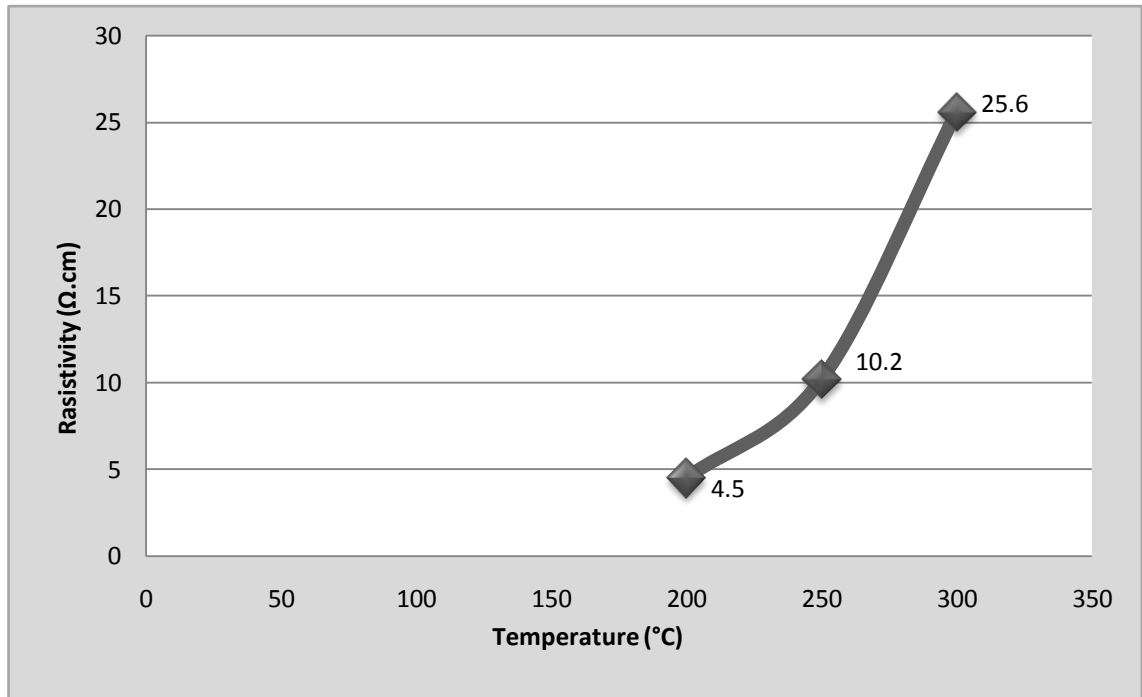


Figure 2.5: Resistivity change due to the different substrate temperature values.

This figure tells that substrate temperature has also significant role to increase the resistivity or sheet resistance values of the  $\text{VO}_x$ .

### 2.3.4 Influence of the Annealing Temperature and Annealing Temperature Duration

Annealing temperature and annealing duration are critical parameters to transform the vanadium oxide into the desired stoichiometry. The obtained vanadium oxide thin film usually consists of several phases. The most common structures in an annealed vanadium oxide thin film are noted as:  $\text{V}_2\text{O}_3$ ,  $\text{VO}_2$ ,  $\text{V}_2\text{O}_5$ , etc [12]. The reason of the formation of these phases depend on the several factors, and it is not clarified exactly yet. On account of this, determining the structures of the material is somewhat difficult.

The main temperature characteristics of these structures are as follows:  $\text{VO}_2$  has a dramatic transition in the electrical and the optical properties around 341.8 K.  $\text{V}_2\text{O}_3$  is a phase owning low phase transition temperature (about 139 K); on the contrary,  $\text{V}_2\text{O}_5$  changes into metallic state at high temperature (about 523 K) [12].

It is already known that increasing the temperature, increases the probability of  $V_2O_5$  occurring in the vanadium oxide [19], however the formations of the other phases are not as precise as  $V_2O_5$ . Therefore, in the studies, achieving the  $V_2O_5$  phase is mostly the prior purpose [19].

Annealing duration is also critical for the resistance change. When the annealing duration increases, it is observed that the resistivity and TCR values measured at 25 °C also increase. The influence of the annealing temperature on the resistances and on the TCR of the resistors is analyzed in Chapter 3 and Chapter 4.

### 2.3.5 Influence of The Argon/Oxygen Flow Rate

Several experiments were carried out to see the influence of the argon/oxygen flow rate. These experiments show that the argon/oxygen ratio is the most important factor to increase the resistivity and the TCR of the vanadium oxide. Table 2.6 shows the sheet resistance change due to oxygen/argon ratio. The effect of the oxygen ratio on the thickness of the films is given in Chapter 3.

The recipe used for the measurements given in Table 2.6 as follows:

- Pressure: ~5.6 mTorr
- DC power: 350 W
- Substrate temperature: 300°C
- No Annealing.

Table 2.6: Change of the resistivity due to oxygen/argon flow ratio.

Sample Number	Oxygen: Argon Flow Rate (sccm)	Average Sheet Resistance ( $\Omega/\square$ )	Average Thickness (nm)	Avg. Resistivity ( $\Omega.cm$ )
7	1.5:15	$0.15 \times 10^6$	139	2
3	3:15	$0.2 \times 10^7$	128	25.6
8	5:15	$0.85 \times 10^9$	120	10.2 k

Figure 2.6 shows the influence of the oxygen partial pressure on the resistivity of the vanadium oxide. As it is seen from the Table 2.6, when the oxygen flow increases the thickness values decrease, however it does not have an effect as much as sheet

resistance changes. In Chapter 3, the difficulties and the problems that are caused by different oxygen ratios are explained in detail.

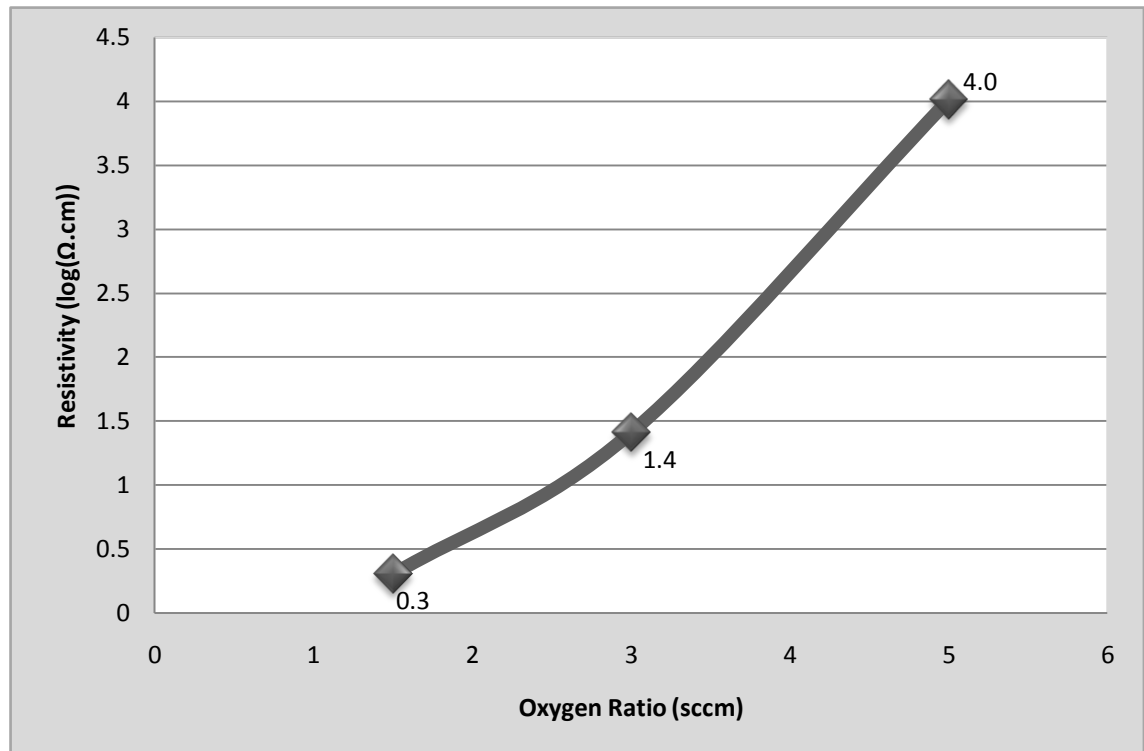


Figure 2.6: Resistivity (logarithmic) change due to the different substrate values.

## 2.4 Conclusion

This chapter presents the processes done before starting the material optimizations and the influences of the sputtering system parameters on the resistivity values of  $\text{VO}_x$ . It is observed that all the parameters of deposition system have an effect on the sheet resistance value of the material, including deposition time, power, deposition temperature, annealing temperature, annealing duration and argon/oxygen ratio. Increasing DC power decreases the resistivity of the  $\text{VO}_x$ . However, the resistivity of vanadium oxide decreases by increasing substrate temperature, annealing temperature or annealing duration, and oxygen ratio of the deposition.

The recipe of Sample 3 is the most compatible recipe to find the proper resistance values for the microbolometers developed in METU. Chapter 3 explains the reason of this compatibility further.

## CHAPTER 3

### FABRICATION AND PROCESS OPTIMIZATION OF THE VO<sub>x</sub> RESISTORS

This chapter presents the optimization work done on the resistor process and the fabrication steps to make a VO<sub>x</sub> resistor. It also reports the problems encountered during these optimizations and in addition to some solutions to prevent these problems. Section 3.1 gives information about the mask and resistor type selection. Section 3.2 presents the determination of the electrode material and the optimization of the etching of the electrodes. Section 3.3 gives all the etching trials of vanadium oxide and their results. It also gives all the recipes that are used in VO<sub>x</sub> depositions to make resistors. Section 3.4 conveys the studies done to optimize the resistance values of the resistors. Finally, Section 3.5 summarizes the results of the resistor trials and concludes the chapter.

#### 3.1 Resistor Type and Mask Selection

The choice of the resistor type is important since it has to be convenient for the resistivity of the active material. There are three types of resistor structures used in the microbolometer studies at METU, namely the planar resistors, the sandwich-gap/sandwich resistors, and the enhanced sandwich type resistors [9]. Among these structures, the most straightforward one is the planar type resistors. In this resistor type, active material layer is formed laterally between the electrodes. Figure 3.1 shows the representative cross sectional view and isometric view of a planar resistor.

Semiconductor YBCO has been used as an active material in the microbolometers fabricated in METU MEMS Center so far. During the experiments, it has been observed that the resistivity of YBCO increases when it is exposed to the atmosphere for extended periods [8]. The resistivity of it is ~120-140 Ω.cm, which rather high compared to that of the VO<sub>x</sub> [20]. To decrease the resistance values of the YBCO

resistors, some other resistor types are developed and used rather than the planar type resistors. Figure 3.2 shows cross-sectional views of sandwich, enhanced-sandwich, and enhanced-sandwich with cover type of resistors.

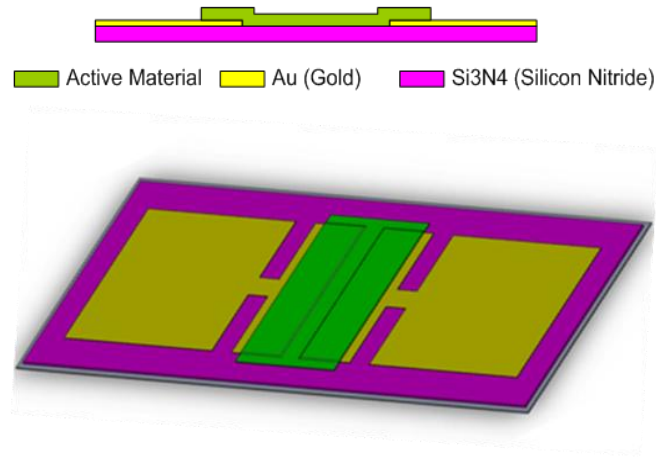


Figure 3.1: Representative cross sectional view of a planar resistor.

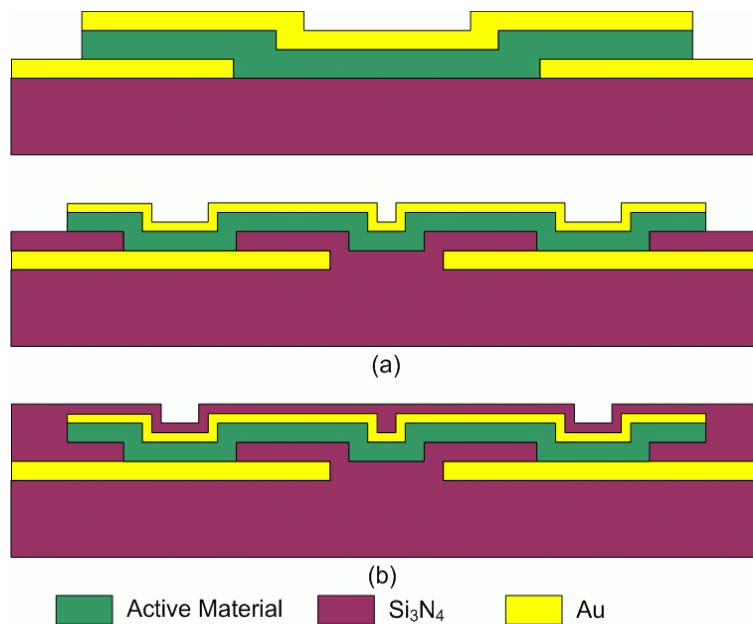


Figure 3.2: Cross sectional view of the three type sandwich resistors: (a) sandwich gap-type resistor, (b) the enhanced sandwich type resistor, and (c) an enhanced sandwich type resistor with a cover layer.

Since the fabrication steps of the planar resistors are fewer than those of the other resistor types, and many samples are required for the optimization processes, vanadium oxide resistors are prepared by using the planar type resistor structures. Figure 3.3 shows the process flow of the planar type resistors.

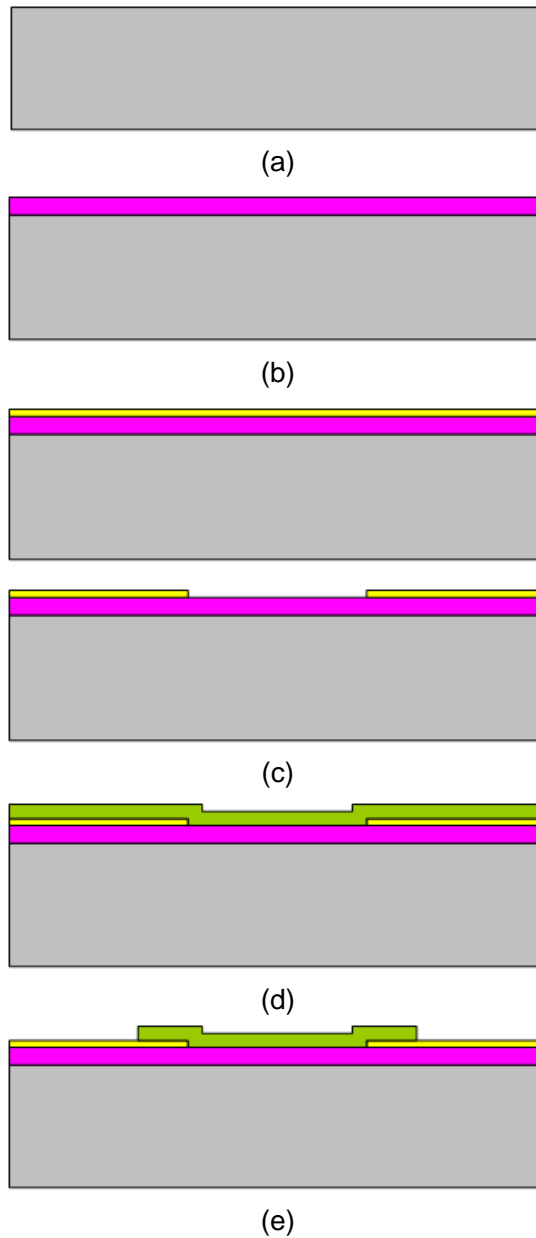
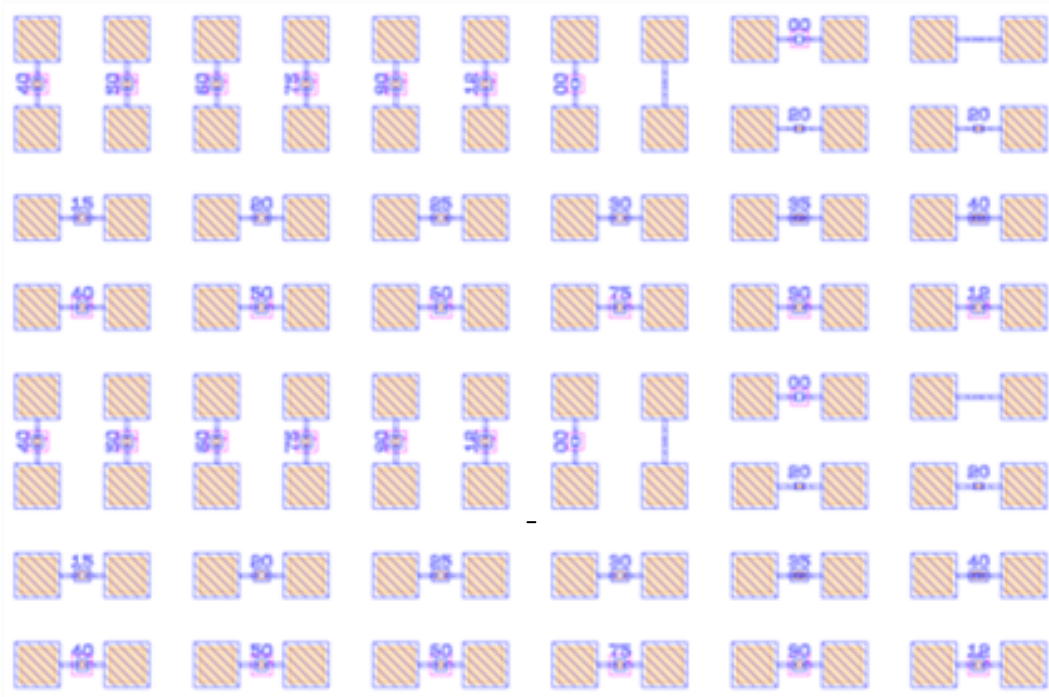
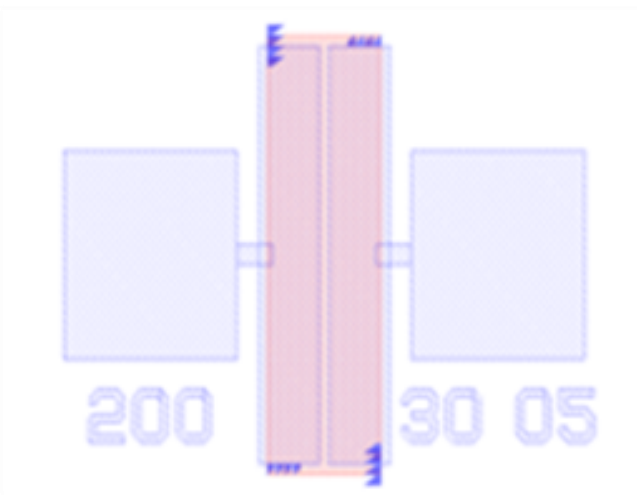


Figure 3.3: Cross sectional view of the process steps in the fabrication flow (a) Silicon wafer. (b) Silicon nitride is coated on silicon sample. (c) Electrode layers are coated and patterned. (d) Active material layer is coated on the electrodes. (e) Active material is patterned.

Planar type resistors can incorporate either straight-planar electrodes or finger type electrodes. The finger type electrodes are used for the high resistivity materials. Still, the most of the structures used in the  $\text{VO}_x$  resistors are straight-planar structures. Figure 3.4 shows these structures along with their representative view.



(a)



(b)

Figure 3.4: (a) Various resistor structures of the 6” resistor mask, (b) a resistor with planar-type electrode.



The resistance of a straight-planar structure is calculated by the aid of the Equation 3.1

$$R = \rho \frac{l}{wt} \quad (3.1)$$

where R is the resistance,  $\rho$  is the resistivity  $l$  is the length, w is the width, and t is the thickness of the resistor.

To optimize the VO<sub>x</sub> resistors, one needs to know the thickness of the active material layer, the resistivity of the film, and the length-to-width ratio of the electrodes should be known. The resistivity and the thickness values of the different processed wafers are given in the Chapter 2. The l/w ratios of the electrodes are measured. The resistance value is calculated by taking all these data into account. During the optimizations, the optimum resistance value, ~70 k $\Omega$ , is tried to be achieved.

Comparison of the resistivity values with the results achieved from the previous chapter shows that the deposition recipe number 3 is the best fitting recipe considering the dimensions of the straight-planar type electrode structures. The resistivity observed with this recipe was 25.6  $\Omega$ .cm. The resistances expected to be observed after fabricating the resistors using this recipe on the straight-planar structures, are changing between 12.5 k $\Omega$  and 125 k $\Omega$  for different structures. Since the results are comparable with the optimum detector resistance range (50-100 k $\Omega$ ) and the average thickness value (~128 nm) is feasible, VO<sub>x</sub> resistor trials are started with this recipe.

## **3.2 Fabrication of the Electrodes**

This section tells the fabrication of the electrodes used in the vanadium oxide resistors.

### **3.2.1 Determination of the Electrode Material**

Determination of the electrode material is important for vanadium oxide processes since the electrodes under VO<sub>x</sub> are also annealed. Annealing in high temperatures might cause sizeable diffusion of materials into one another which is observed in the VO<sub>x</sub> resistors.

### 3.2.1.1 Gold with Adhesion Layers

Gold is used often in MEMS processes. However, since thin film gold has problems adhering to silicon or silicon nitride, a thin titanium or chromium film is used as an adhesion metal underneath the gold film.

The first trials with gold and titanium showed that after the annealing step of vanadium oxide, the titanium layer diffused into the gold layer. The diffusion is also observed as a numerous small particles similar as contamination on the surface of the electrodes. Moreover, these particles prevent good contact between electrode and vanadium oxide surfaces. The problem is dealt further studies, as given in the following chapters. Figure 3.5 shows a resistor after the lithography step of  $VO_x$ , there exists gaps and dots on the electrode surfaces.

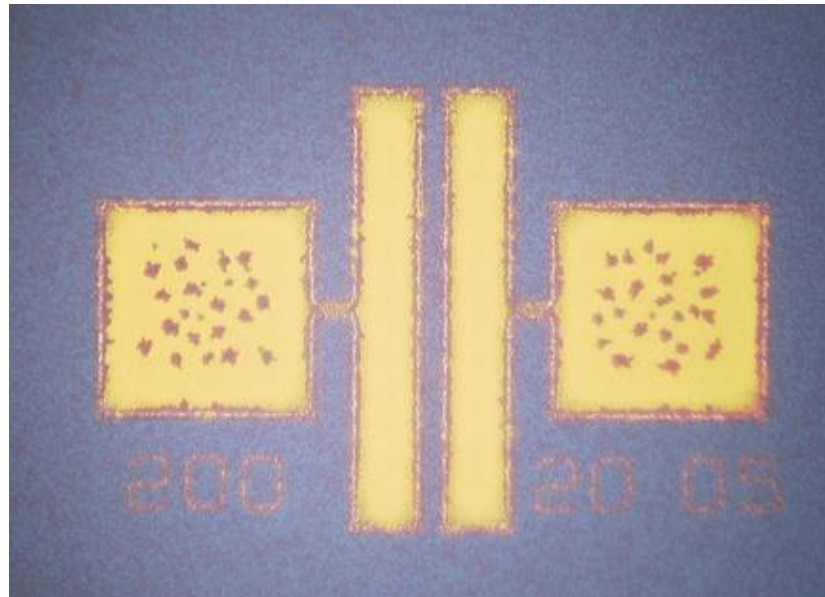


Figure 3.5: Titanium diffuses into gold, during the depositions at high temperatures.

To overcome this problem, chromium is used as the adhesion layer but the problems have continued. The dots and the gaps on the electrodes occur most likely due to the long annealing duration of vanadium oxide. High temperatures increase the reaction of the surface materials and cause the materials to diffuse into each other. Figure 3.6 shows the chromium/gold coated electrode. Apparently, the dots on the electrodes still persist.

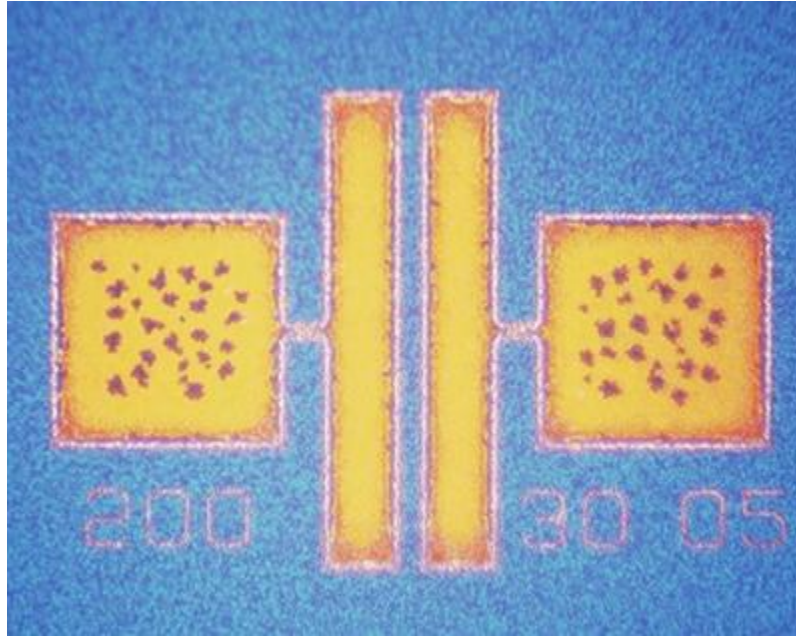


Figure 3.6: Chromium diffuses into gold, during the depositions at high temperatures.

### 3.2.2 Etching Optimization of the Gold Electrodes

There are two options for the etching of the gold electrodes: wet etching and Metal RIE. Metal RIE is a type of plasma etching, so it is more selective than the wet etching. However, wet etching is frequently used etchant type in the resistor trials in METU and its optimizations had been done before [20]. Therefore, etching of the electrodes of the  $VO_x$  resistors is started with wet etching. There is a commercial (TFA) etchant of gold by Transene Company which is used in some MEMS processes. However, diluted Aqua Regia is preferred over the TFA etchant because of its lower etch rate. The formula of this etchant is  $H_2O:HCl:HNO_3$  (5:2:1). To pattern  $0.5\ \mu m$  openings, S1805 type photoresist is used. This type of photoresist (PR) has a comparably lower viscosity which allows thinner coatings. In the exposure step, the finger spacing is opened successfully with S1805. On the contrary, using S1813 photoresist, which has a higher viscosity, causes the already narrow fingers to be obliterated after lithography. As previously mentioned in Section 3.1, straight-planar electrodes have been used for the resistor structures. Since the openings are much higher than the openings in finger type electrodes, S1813 photoresist can be used for these types of electrodes. Figure 3.7 shows the straight-planar electrodes formed by wet etching and by using S1813 photoresist in the lithography.

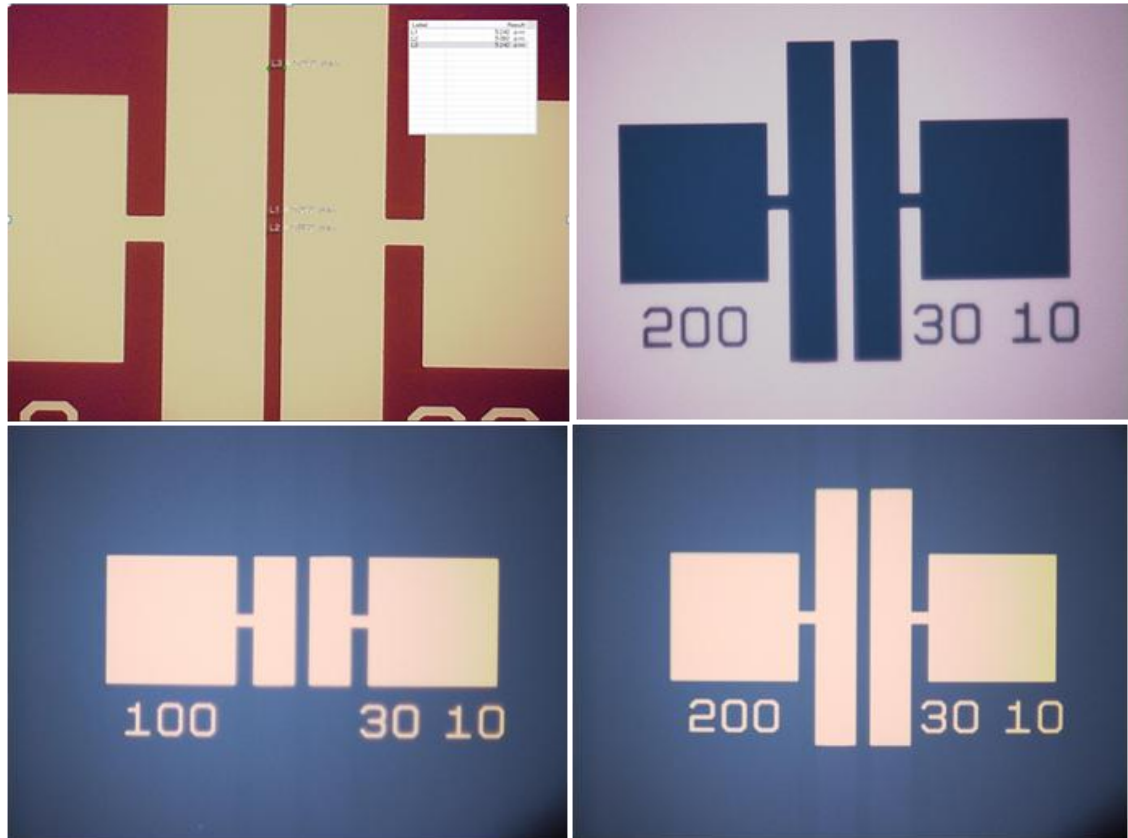


Figure 3.7: Various straight-planar electrodes formed by wet etching.

Although wet etching is an option to etch straight-planar structures, 0.5 or 0.7  $\mu\text{m}$  openings in the finger type electrodes cannot be successfully patterned. Metal RIE has an active role in this part. However, the etching optimizations of the finger electrodes in Metal RIE need further studies.

The Metal RIE method is used to pattern the finger electrodes. To prepare a wafer to be etched in metal RIE, firstly, chromium is coated as the adhesion layer, gold is deposited on it, and then a very thin (15-20 nm) titanium layer is coated directly on the photoresist.<sup>(1)</sup> At the beginning of the Metal RIE optimizations, it is seen that gold is sputtered on the walls of the etching areas, as a solution to prevent this, thin film titanium is covered on the gold. Figure 3.8 shows the gold walls on the sides of the openings due to the physical etching of gold in Metal RIE.

<sup>1</sup> This approach is developed by Mr. Akin Aydemir.

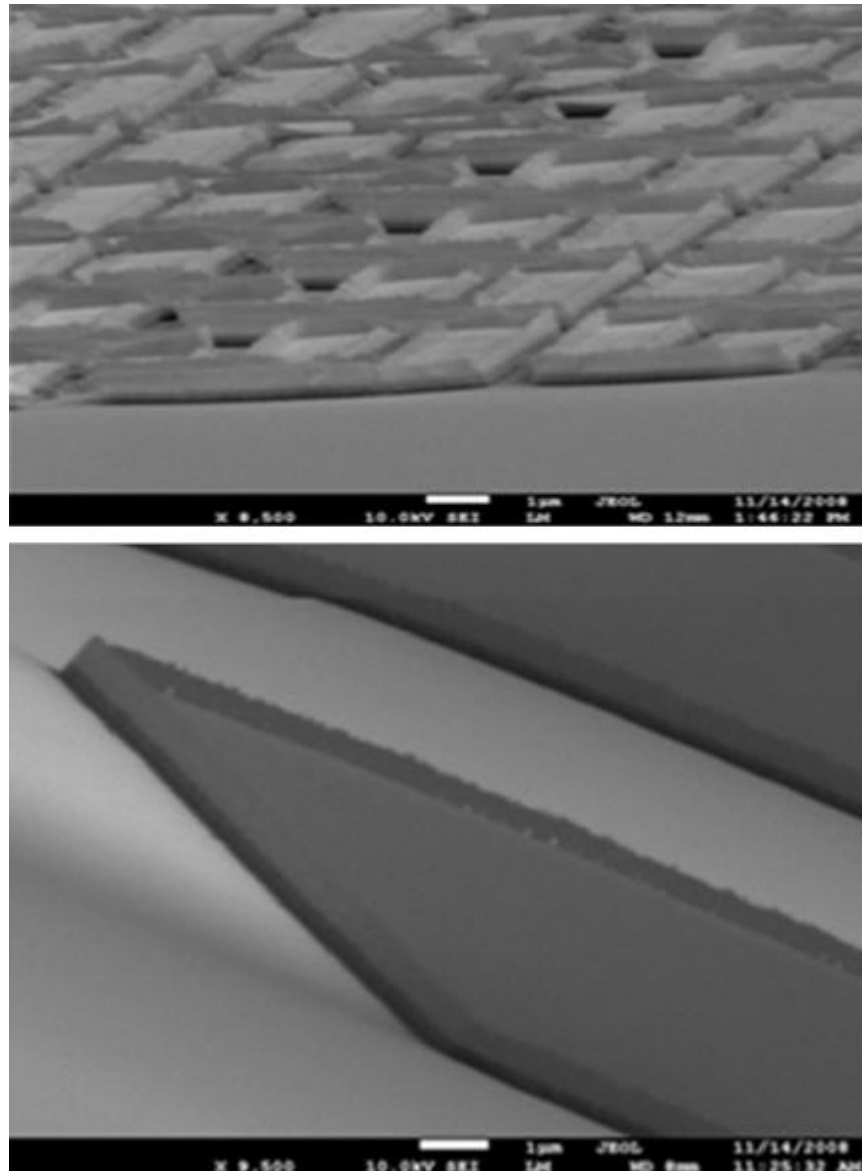


Figure 3.8: Gold walls are occurred on the sides of the openings due to the physical etching of gold in Metal RIE.

Moreover, during the optimization of the etching process, it is seen that the photoresist cannot be deposited thick enough to withstand the etching and permit the patterning of fine structures at the same time. Consequently, if the gold etching process is done by the Metal RIE system without the additional thin titanium layer, the photoresist is etched, and the resultant structures are distorted. Figure 3.9 shows the lastly achieved Metal RIE optimizations of the finger electrodes.

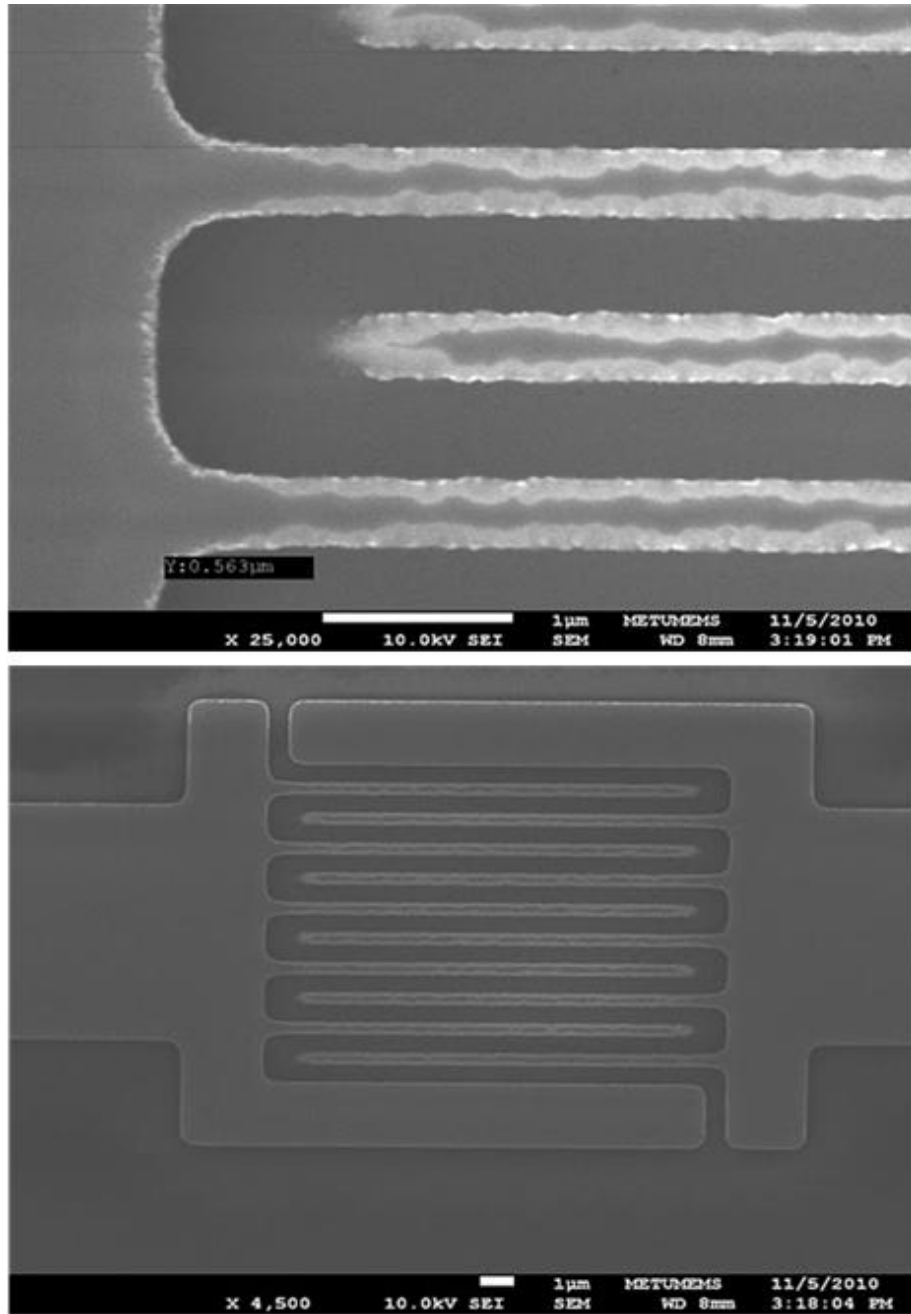


Figure 3.9: The results of the finger electrode etching trials with metal RIE. Fingers are made of 20 nm Cr and 50 nm Au layers, and 0.5µ Ti is coated on the photoresist. Etch duration: 50 sec, gas used: Ar and HBr<sup>(2)</sup>.

<sup>2</sup> All the Metal RIE processes in this thesis are done by the help of Mr. Akın Aydemir, and the SEM photos are also taken by the help of him.

### 3.2.3 Etching optimization of the Platinum Electrodes

Up to now, gold has been used as an electrode material in METU MEMS Center facilities. However, there are more opportunities rather than gold, as the electrical contact metal. One of them is platinum. Considering this, platinum is tried to be optimized as an electrode layer. Significant numbers of experiments are carried out to understand the Pt characteristics and all the experiments are told below. The studies on the etching of the platinum are not completed yet. In the future, these etching trials will be carried on.

The experiments with platinum are started with the resistivity measurements of the platinum, and then the thickness non-uniformity test of the target is done. At last, the preparation of the samples to optimize the etching of platinum is done. Platinum is deposited by the magnetron sputtering method on silicon nitride coated wafers.

The durability of platinum is very high compared to gold [21]. This property of the platinum makes it a difficult material to etch. In the literature there are many methods for Pt etching [22]. In these methods, the most effective ones are hot Aqua Regia solution, and dry etching. Figure 3.10 shows the platinum electrode structure, after etching trial of Pt in aqua regia solution.

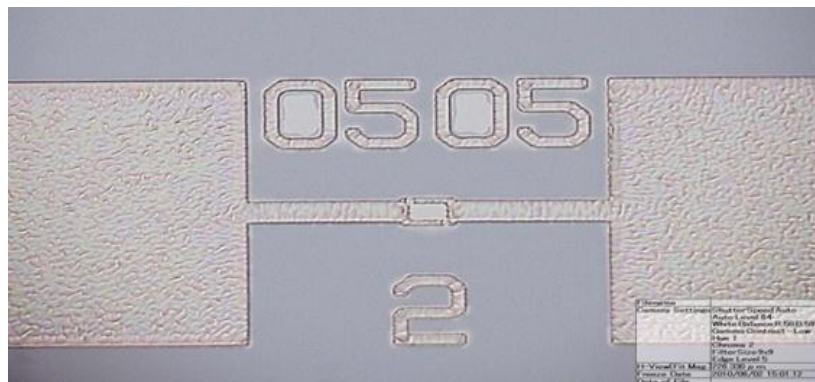


Figure 3.10: Pt is not etched by the Aqua Regia solution annealed at 100 °C.

By changing the HCl or H<sub>2</sub>NO<sub>3</sub> amounts in the aqua regia, some more trials achieved, but any of them did not work to etch Pt exactly. It usually takes a long time to increase the temperature of the solution on the hotplate which causes the solution to be degraded in the process. Moreover, the method of heating the etching solutions is very risky.

After observing the results of the trials with wet etching, Metal RIE is carried out to etch Pt. Figure 3.11 gives SEM photos of the etched Pt coated sample taken after the metal RIE process. While  $0.7\ \mu$  openings of the finger electrodes are opened well,  $0.5\ \mu$  fingers are over etched. The recipe used as follows: time: 60 sec, gas: Ar. To strip the photoresist, 1 hour oxygen plasma, 20 minutes PRS are done.

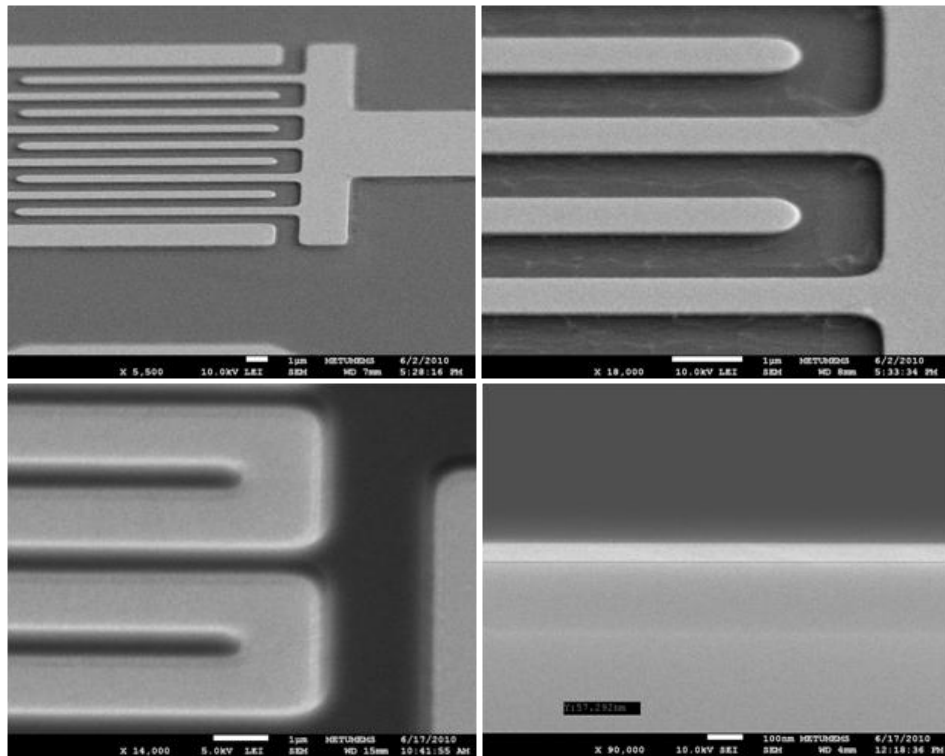


Figure 3.11: After 60 seconds etching by metal RIE of the 60 nm thick Pt finger electrodes.

As seen from the SEM images, platinum can be etched by Metal RIE. Still it needs to be optimized further. The etching results may change by using Cr or Ti under Pt, and it might be necessary to deposit titanium directly on the patterned PR as explained before. Further, to replace the gold with the platinum in the  $\text{VO}_x$  resistor structures, the material characteristics of the platinum should be observed after  $\text{VO}_x$  is deposited on it at  $300^\circ\text{C}$  whether to see it is affected from the temperature as much as gold or not. The optimizations of the etching of the platinum by Metal RIE could not be continued due to some problems in the deposition chamber of the platinum target.



### 3.3 Etching Optimization of the VO<sub>x</sub> Resistors

Etching optimization of the VO<sub>x</sub> resistors is started with VO<sub>x</sub> deposited silicon-nitride wafers. In the literature, a large number of the vanadium oxide etching methods is given [7, 23] Among these, TFN solution and dry etching are the most popular ones. Some of the groups make the VO<sub>x</sub> etchings by hydrogen peroxide (H<sub>2</sub>O<sub>2</sub>) solutions [23]. The deposition recipe used for the etching trials given in Table 3.1 is as follows:

- Pressure: ~6 mTorr
- O<sub>2</sub>:Ar flow: 1.5 : 45
- Deposition Time: 2000 sec.
- Substrate temperature: 210°C, no annealing.
- DC Power: 450 W

As it is seen from the table, the best etching method for the prepared vanadium oxide thin films is wet etching by hydrogen peroxide. Even a small amount of hydrogen peroxide solution, etches low oxygen doped vanadium oxide perfectly.

At the end of the etching of VO<sub>x</sub> thin films, the etching trials of the resistors were started. Firstly, etching trial of the resistors deposited with the recipe achieved in Chapter 2, are done. After the lithography step of this trial, it is observed that vanadium oxide is completely etched with developer. In the trials given in Table 3.1, photoresist developer did not etch the VO<sub>x</sub>, because the oxygen ratio of the VO<sub>x</sub> deposition recipe is low and the samples are not annealed during the deposition process, the reason of this will be discussed in detail in this chapter. Figure 3.12 shows the resistor sample that is totally etched by the developer. The dots and gaps explained in the previous chapter are seen in this resistor sample also.

In the literature, it is mentioned that V<sub>2</sub>O<sub>5</sub> phase of vanadium oxide can be etched by the photoresist developers [24]. Since the oxygen ratio is very high in this process, as mentioned before, it is most likely that majority of the VO<sub>x</sub> transformed into V<sub>2</sub>O<sub>5</sub> phase. The problem stems from the deposition recipe of the vanadium oxide. After decreasing the oxygen ratio during the deposition, this problem is solved. It is understood that 15:3 (Ar: O<sub>2</sub>) flow recipe is a highly oxygen doped one. This makes the

$V_2O_5$  phases in vanadium oxide form. However, not only the oxygen doping, but also annealing temperature and annealing durations are the other factors to make this phase.

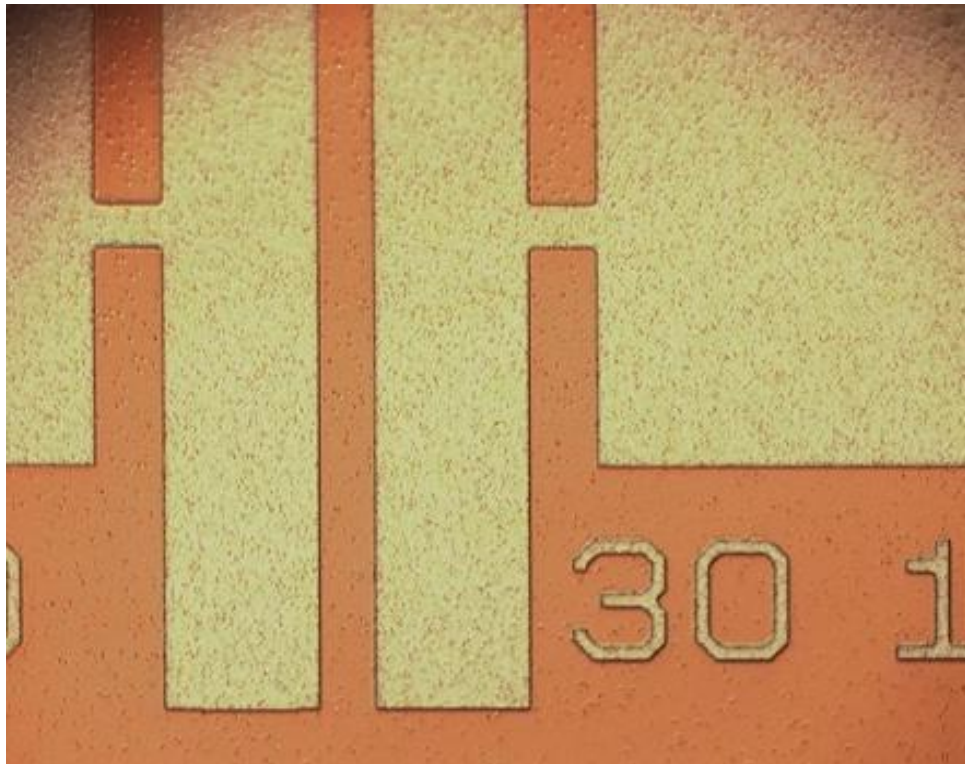


Figure 3.12: A closer look to the resistor sample that is prepared with the recipe of Sample 3 given in Chapter 2.

The material characterization results of the samples prepared in both conditions are given in Chapter 4. These results changed the course of the study. In the literature, there are studies that deposit  $VO_x$  in very low oxygen ratios like 30:1 or 30:1.5 (Ar: $O_2$ ) flow rates [19]. Moreover, in some of them, high TCR values are achieved after deposition by annealing the samples. Since our main purpose is to achieve a good TCR with  $VO_x$  resistors, low resistance values achieving good TCR will not affect our work. That is because resistor structures can be redesigned to be appropriate for that newly found  $VO_x$  recipe. After considering all these parameters and their consequences,  $VO_x$  studies were categorized into not-annealed and low oxygen doped, and not-annealed and high oxygen doped, annealed and low oxygen doped, annealed and high oxygen doped groups.

Table 3.1: Etching trials of the prepared vanadium oxide thin film.

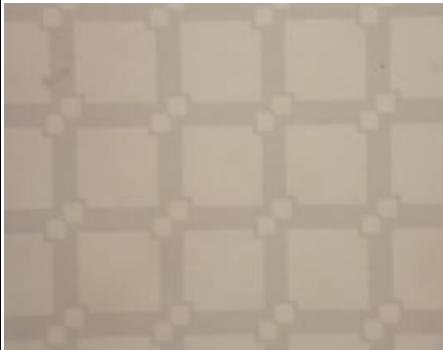

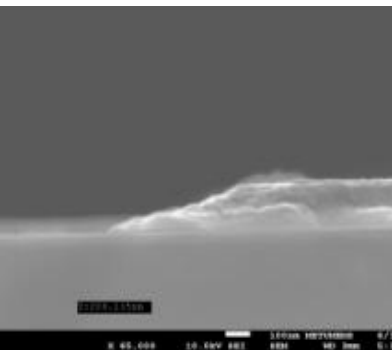
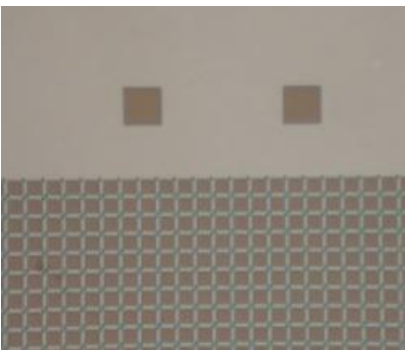
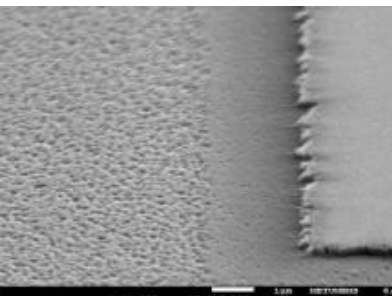
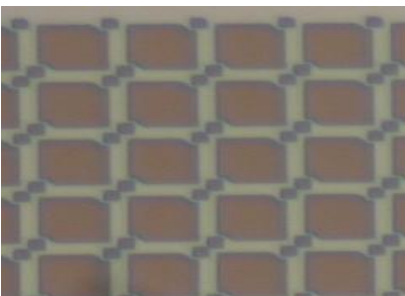
PHOTORESIST STRIP METHOD						
ETCHING TRIAL	Acetone	Oxygen Plasma	PRS 1000 (@80°C)	SVC (@80°C)	SEM Results	Inspection After the Etching Trials
Diluted HCl Acid	Done				Etch did not finish	 PR Stripped Totally
Diluted Nitric Acid	Done				Etch did not finish	 PR Stripped Totally

Table 3.1 (continued): Etching trials of the prepared vanadium oxide thin film.

PHOTORESIST STRIP METHOD						
ETCHING TRIAL	Acetone	Oxygen Plasma	PRS 1000 (@80°C)	SVC (@80°C)	SEM Results	Inspection After the Etching Trials
Diluted H <sub>2</sub> O <sub>2</sub>	Done	Done	Done		 <p>Undercut</p>	
Diluted H <sub>2</sub> O <sub>2</sub> + HF				Done	 <p>Undercut + Rough Surface</p>	

### 3.3.1 Not annealed-Low Oxygen Doped Resistors

Table 3.2 shows the VO<sub>x</sub> deposition recipes for all “not annealed-low oxygen doped” trials. Figure 3.13 shows some of the results of these trials. While the resistors of the Sample 6 are over-etched, the resistor of the Sample 3 is etched better.

Table 3.2: Some of the VO<sub>x</sub> deposition recipes of the “not annealed-low oxygen doped” resistors.

Resistor Sample Number	Substrate Temperature	Ar:O <sub>2</sub> Flow (sccm)	Deposition Time (seconds)	Pressure (mTorr)	DC Power (W)	Annealing
1	300 °C	1.5 : 15	1000	~6	450	None
2	300 °C	1.5 : 15	1500	~6	450	None
3	300 °C	1.5 : 25	500	~6	450	None
4	250 °C	1.5 : 25	500	~6	450	None
5	250 °C	1.5 : 20	500	~6	450	None
6	325 °C	1.5 : 25	3300	~6	450	None

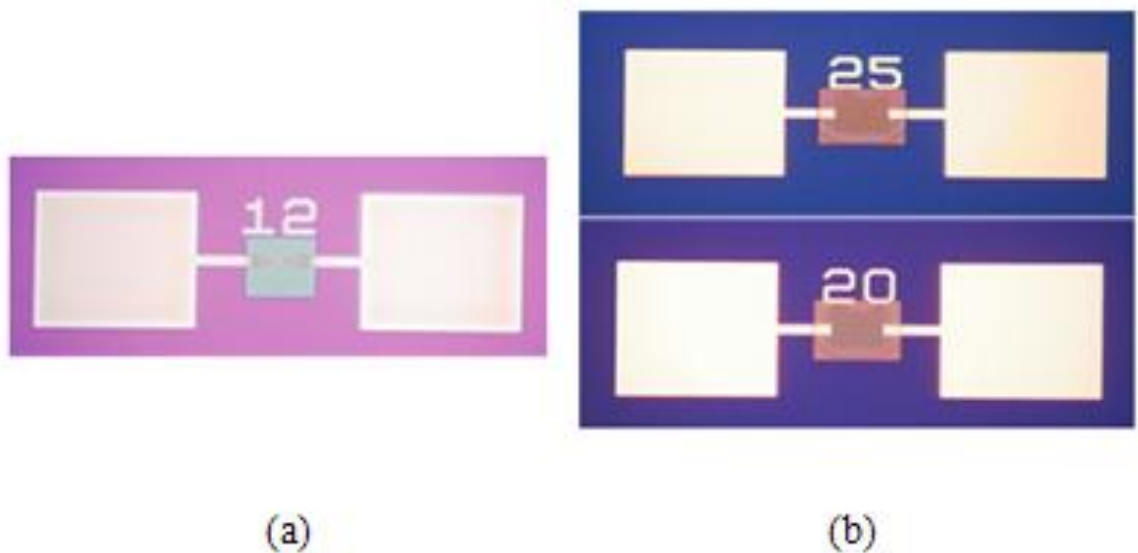


Figure 3.13: The resistor samples after etching trials: (a) a structure from the resistor Sample 3 given in Table 3.2, the photoresist is stripped, and (b) the structures from the resistor Sample 6 of which the vanadium oxide layer is over etched, the photoresist still remains after etching.

In these trials, the developer does not remove vanadium oxide, which means it does not include  $V_2O_5$  phase in its form as it is discussed before. The etchings of all these resistors are successful. Resistor structures of the “not annealed-low oxygen” recipe are etched by the diluted hydrogen peroxide ( $H_2O_2 : H_2O, 1 : 2$ ).

### 3.3.2 Not Annealed-High Oxygen Doped Resistors

The deposition recipes of the “Not Annealed-High Oxygen Doped Resistors” are given in the Table 3.3. All these samples are also etched by the developer, but the etching rate is not as much as the ones in the high oxygen doped-annealed group. In some of the samples in this group, vanadium oxide layer still stays; the photoresist layer protects the vanadium oxide layer. Some of them are totally etched by the developer very quickly. Figure 3.14 shows the sample resistors totally etched by the PR developer.

Table 3.3: Some of the  $VO_x$  deposition recipes of the “not annealed-high oxygen doped” resistors.

Resistor Sample Number	Substrate Temperature	Ar:O <sub>2</sub> Flow (sccm)	Deposition Time (seconds)	Pressure (mTorr)	DC Power (W)	Annealing
7	300 °C	3 : 15	1500	~5.6	450	None
8	300 °C	4 : 15	1000	~5.6	450	None
9	300 °C	4 : 10	2000	~5.6	450	None
10	300 °C	7.5 : 15	2000	~4.5	450	None
11	300 °C	7.5 : 15	1000	~4.5	450	None

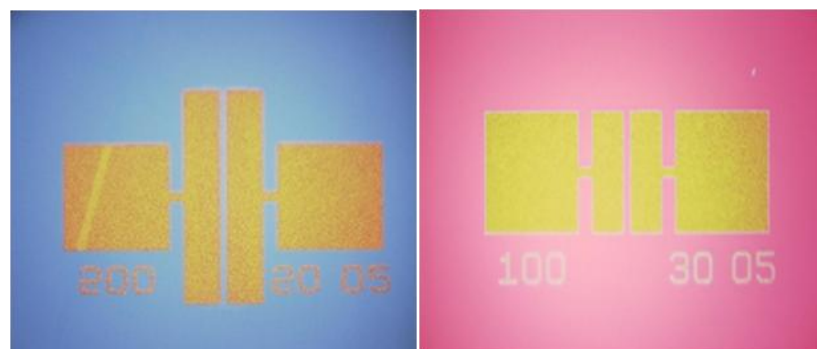


Figure 3.14: Some of the resistor samples from the sample wafer 9 and 10, respectively. The vanadium oxide layers are totally etched by the developer.

### 3.3.3 Annealed-Low Oxygen Doped Resistors

In these resistors, the photoresist developer does not etch the vanadium oxide, but other problems continued. After the etching of the vanadium oxide film, the dots and points on the electrodes are observed clearly, which means the diffusion problem occurred again. Table 3.4 gives the trials prepared in this group, and Figure 3.15 shows the images of the resistors prepared with these recipes.

Table 3.4: Some of the VO<sub>x</sub> deposition recipes of the “annealed-low oxygen doped” resistors.

Resistor Sample Number	Substrate Temperature	Ar:O <sub>2</sub> Flow (sccm)	Deposition Time (seconds)	Pressure (mTorr)	DC Power (W)	Annealing Duration
12	300 °C	1.5 : 15	1500	~6	450	1 h
13	300 °C	1.5 : 15	2000	~6	450	40 min
14	300 °C	1.5 : 25	500	~6	450	30 min

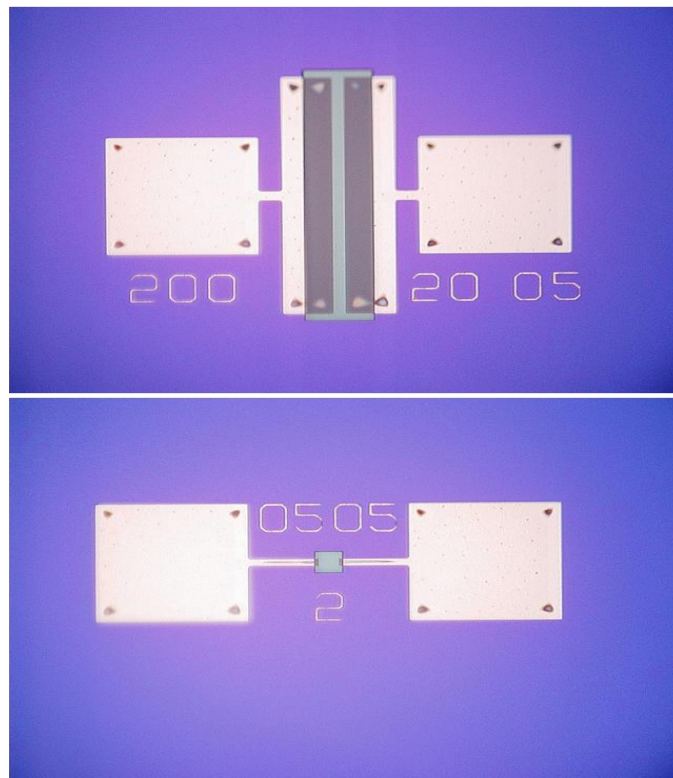


Figure 3.15: Resistors of Sample 14, after etching step of the vanadium oxide layer.

The resistors given in Figure 3.15 are etched by the diluted hydrogen peroxide ( $\text{H}_2\text{O}_2$ :  $\text{H}_2\text{O}$ , 1:2), however the effect of the annealing is seen on the electrodes.  $\text{VO}_x$  on the electrodes are not etched and the surfaces of the electrodes are not cleaned enough.

### 3.3.4 Annealed-High Oxygen Doped Resistors

The trials of the “annealed-high oxygen doped” resistors are given in Table 3.5. In all these trials,  $\text{VO}_x$  is etched by the photoresist developer abruptly. Figure 3.16 shows a resistor from Sample 15, it is seen from the figure that  $\text{VO}_x$  is etched totally by the PR developer. Moreover, because of the annealing effect, a contamination layer occurred on the electrodes of the resistor.

Table 3.5: Some of the process recipes of the “annealed-high oxygen doped” resistors.

Resistor Sample Number	Substrate Temperature	Ar:O <sub>2</sub> Flow (sccm)	Deposition Time (seconds)	Pressure (mTorr)	DC Power (W)	Annealing Duration
15	300 °C	3 : 15	1500	~5.6	450	1 h
16	300 °C	4 : 15	1500	~5.6	450	40 min
17	300 °C	4 : 10	2000	~5.6	450	40 min

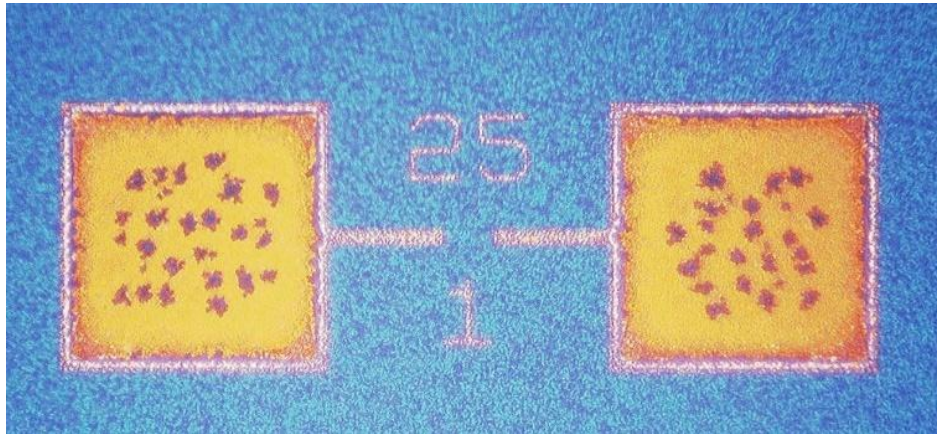


Figure 3.16: A resistor from the sample 15, inspected after the lithography of the vanadium oxide layer.  $\text{VO}_x$  is totally etched by the photoresist developer.

To prevent the etching of the vanadium oxide in the developer and the contamination on the electrodes, a new process flow is employed. Figure 3.17 shows the cross section of this new process flow.



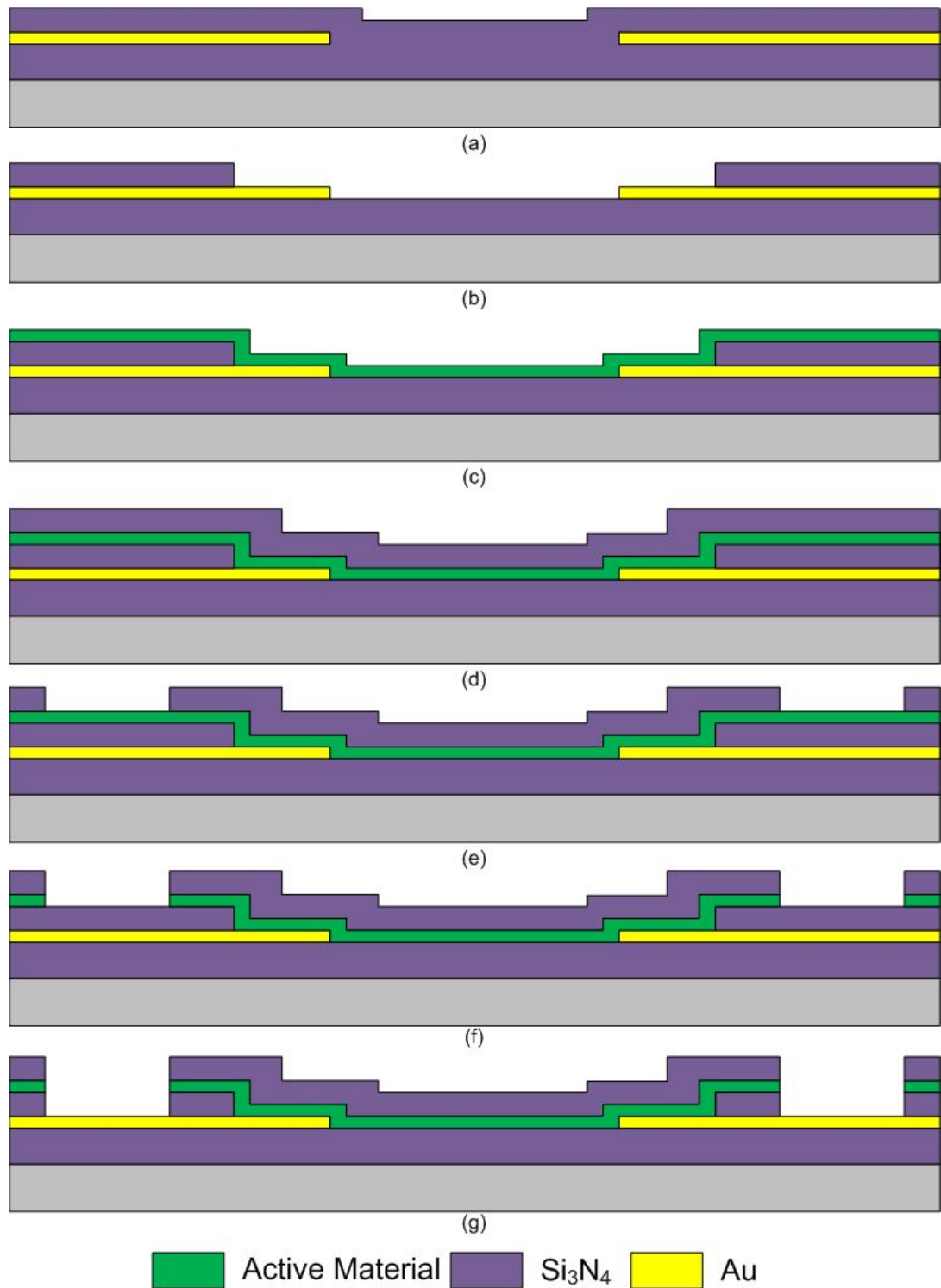


Figure 3.17: (a) To prevent the contamination problem on gold, silicon nitride layer is coated on the gold electrodes first. (b) Then, silicon nitride is opened in the middle of the electrodes. (c) Vanadium Oxide active material layer is deposited after. (d) Silicon nitride is coated on the  $\text{VO}_x$  active material. (e) Then the silicon nitride layer is etched. (f) Vanadium Oxide layer is etched. (g) Last nitride layer is etched.

In this process flow; the first nitride layer on the electrodes prevents the contamination on the electrodes. The contact between the surfaces of the vanadium oxide and the gold is blocked. The second nitride layer is coated on the vanadium oxide layer to prevent the vanadium oxide from the etching of the photoresist developer. Figure 3.18 shows some of the steps processed by the following process flow.

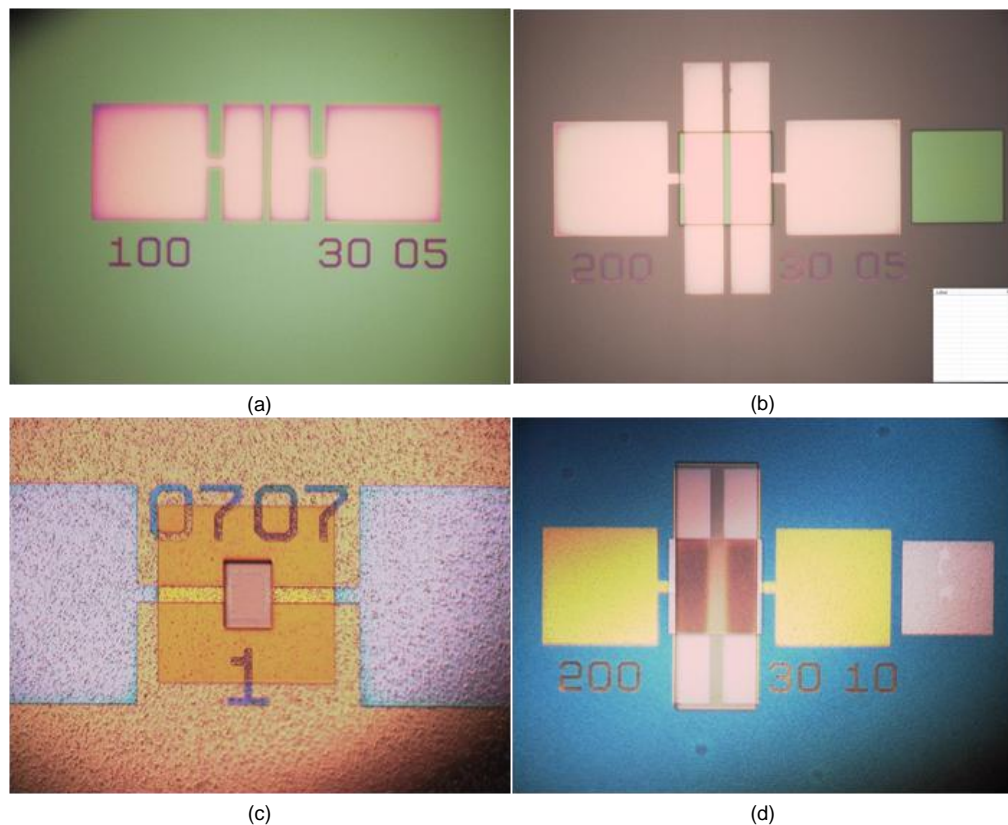


Figure 3.18: Some of the process steps of the new process flow: (a) After silicon nitride is coated on the electrode layer, (b) after photoresist development of the nitride layer, (the layer in the middle is opened), (c) after the development of the  $VO_x$  layer, which is in the middle of the electrodes, (d) after the etching of the  $VO_x$ , the last step of the new process flow.

This process is not succeeded in the first time tried. The etching time of the silicon nitride could not have been optimized. Since the contact openings are not entirely opened, electrical measurements of these resistors cannot be done. Due to some problems with the PECVD, the optimization of this new process could not be finalized.

### 3.4 Optimization of the Resistance Values

The optimum resistance values for the microbolometers fabricated at METU should be achieved for proper operation. However as shown in the previous section, when the best optimization result given in Chapter 2 is used in the resistor structures, some problems are encountered.

When the resistances are measured throughout the four different groups of resistors told above, the resistance values are observed lower or much higher than the desired values. The resistances of the not-annealed-low oxygen doped resistors are too low ( $\sim 0.3 \text{ k}\Omega$ ). The vanadium oxide layers of the annealed and high oxygen doped ones are mostly eaten by the developer. However, the resistances of the other group resistors are not reliable; their resistances are changed after the bonding step which is necessary for TCR and noise measurements. Figure 3.19 shows a sample in the course of the resistance measurement by the probe station.

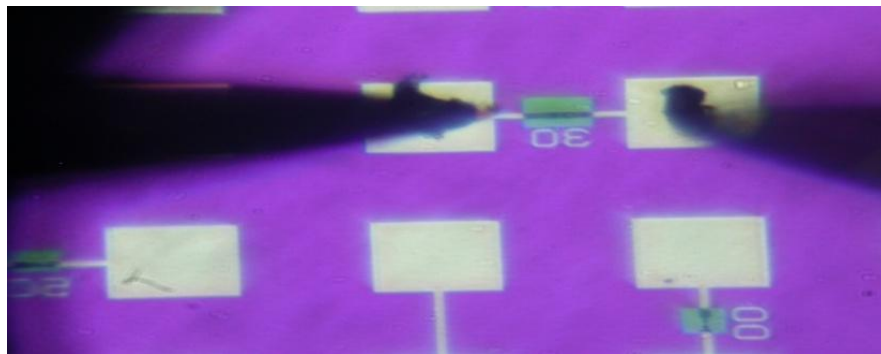


Figure 3.19: Resistance measurements are made by the probe station in the clean room.

The main problem in the resistors is the material remaining on the electrodes. This causes all the electrical measurements to fail. Although some of the resistances of the electrodes are measured to be very low ( $10\text{-}100 \Omega$ ), after wire bonding to the contact surfaces of the resistors to make TCR or noise tests, the resistances increased instantly. The problem probably occurs due to the inherent annealing during the bonding (the curing phase of the epoxy). Even though the contamination occurs on the electrode is very thin and seems like metal, bonding causes a sudden change and increases the resistances. A sudden increase in the temperature might change the phase of the material.

As a result, resistance optimizations are divided into two groups: In the first group, there are resistance values which are too low compared with the optimum values (50-100kΩ) of the microbolometers, the second group consists of the very high resistance values, when they are again compared with the proper range.

### 3.4.1 Low Resistance Group

There are many studies on the literature which use low resistivity vanadium oxide films, furthermore, the TCR values given in these studies are high enough (2-2.5 %/K) [14]. However, in this study, it is observed that the TCR values of the low resistive resistors are too low. The TCR results of the resistors with low resistances are given Chapter 4.

There are also studies in which the resistivity and the TCR of the VO<sub>x</sub> films are increased by annealing method [25]. However, in some vanadium oxide studies, it is claimed that vacuum annealing decreases the resistivity values, and increases the TCR values [26]. In this study, vacuum annealing did not change the resistance values. It is observed that annealing on hot plate increases the resistances of the resistors.

Table 3.6 shows the change of the resistances of different samples after annealing process. As it is seen from the table, the resistances of the samples are not increased at the same rate in 15 minutes, in the annealing trials, this state is observed several times.

Table 3.6: The changes of the resistances after different annealing recipes.

Resistor Sample (in Table 3.2)	Annealing	Duration (min)	Annealing Temperature (°C)	Initial Resistance (kΩ) @ 25°C	Final Resistance (kΩ) After Annealing @ 25°C (w/1 of the resistors= $\sim$ 16)
2	on hotplate	15	300	$\sim$ 2.2	$\sim$ 164
3	on hotplate	15	300	$\sim$ 2.3	$\sim$ 230
3	on hotplate	15	50	$\sim$ 2.3	$\sim$ 350
3	on hotplate	30	50	$\sim$ 2.3	$\sim$ 401

After annealing, and after increasing the resistances and making the resistance values suitable with the current noise setup at METU, noise and TCR measurements of the resistors are done. Some of these measurements are given in Chapter 4.

### 3.4.2 High Resistance Group

Most of the recipes tried in the deposition of  $VO_x$  resulted in very high resistances. To decrease the resistances of these resistors, some of them are deposited thicker. Table 3.7 gives the resistance values corresponding to the deposition recipes of  $VO_x$ . For achieving TCR measurements, resistances should be much lower than these values.

Table 3.7: The resistance measurement results of the some trials. The resistances are over the range of the desired resistance range (50-100 k $\Omega$ ).

Resistor Sample (in Table 3.3)	Initial Deposition Time	Initial Resistance(M $\Omega$ ) @ 25°C	Increased Deposition Time	Final Resistance After Annealing @ 25°C (w/1 of the resistors= $\sim$ 16)
10	2000	open	7200	$\sim$ 50 M $\Omega$
10	2000	open	21600	$\sim$ 45 M $\Omega$
8	1000	50 M $\Omega$	7200	$\sim$ 3.5 M $\Omega$
8	1000	50 M $\Omega$	14400	$\sim$ 1.2 M $\Omega$

All the resistors given in Table 3.7 are etched by the PR developer. When the deposition time of the resistor 10 is increased to 7200 sec, the resistances decrease to 50 M $\Omega$ , however when the deposition time increased 3 times higher, the resistances do not decrease at the same rate. The same process is applied to the resistor sample 8, and as it is seen from the table, the 3.5 M $\Omega$  resistances are decreased to 1.2 M $\Omega$  values. After increasing the deposition time, at the same rate with the deposition time, the resistances are decreased. To decrease the resistances more, the deposition time is increased more, however, this time the vanadium oxide layer is etched by the PR developer totally

again. Since, the experiments done to decrease the resistances are failed, the TCR or noise measurements of these resistors cannot be made.

### **3.5 Conclusion**

This chapter presented all of the processes done to make a vanadium oxide resistor. It described the optimization of the electrode in the resistors and gave all the experiments for the optimization of the etching of different vanadium oxide forms.

The problems occurred during the etching of the  $\text{VO}_x$  are examined in detail. The contamination problem of the resistors are seen in all “high doped” or “annealed” samples. On the other hand, while the “low doped” and “not-annealed” samples are etched easily with diluted hydrogen peroxide, most of the others are etched by the PR developer. Since the etching occurs in a very short period, there is no possibility to control the etching of the vanadium oxide by the PR developer.

The resistances of the resistors prepared are measured, but their resistances are not reliable because of the contamination on the electrodes. After the resistors are wire bonded for the TCR or noise measurement tests, the resistances changed in some of the samples. Both annealing process to increase the low resistance values, and thicker depositions, to decrease the high resistance values of the resistors did not work.

To get rid of all these problems, a new process flow is designed, the optimization of the process is started, but it could not have been continued due to some unexpected difficulties encountered in the clean room facilities.

# CHAPTER 4

## CHARACTERIZATION AND TEST RESULTS

This chapter presents the characterization and test results of the some vanadium oxide samples which will clarify the effects of the annealing and oxygen doping during the VO<sub>x</sub> deposition. Section 4.1 states the characterization measurements of the material, gives the XRD and XPS results of the VO<sub>x</sub> samples that should be particularly examined. Section 4.2 gives the TCR and the noise measurement results of these samples. Section 4.3 concludes and briefly summarizes the chapter.

### 4.1 Characterization Results

During the VO<sub>x</sub> development, it is clearly observed that increasing oxygen in the recipes is making the material more resistive. Studies on VO<sub>x</sub> in the literature support this case. The resistivity increase is explained by the V<sub>2</sub>O<sub>5</sub> phase transformation in the VO<sub>x</sub> structure. At the same time, increasing oxygen in the structures makes the same effect and increases the V<sub>2</sub>O<sub>5</sub> phase in the form of VO<sub>x</sub>. To see the phase transformations, one of the “not-annealed and low oxygen doped”, and one of the “not-annealed and high oxygen doped” recipes are chosen, and by using those deposition recipes, samples for the XRD measurements are prepared. Table 4.1 lists the different deposition recipes applied to VO<sub>x</sub> samples for XRD measurements. Figure 4.1 presents the XRD measurement results of the samples.

Table 4.1: Different recipes applied to VO<sub>x</sub> samples for XRD measurements.

Sample Number	Substrate Temperature	Ar:O <sub>2</sub> Flow (sccm)	Deposition Time (seconds)	Pressure (mTorr)	DC Power (W)	Annealing Duration
1	300 °C	1.5 : 15	1500	7	450	none
2	300 °C	1.5 : 15	1500	7	450	1 hour
3	300 °C	3 : 15	1500	7	450	none

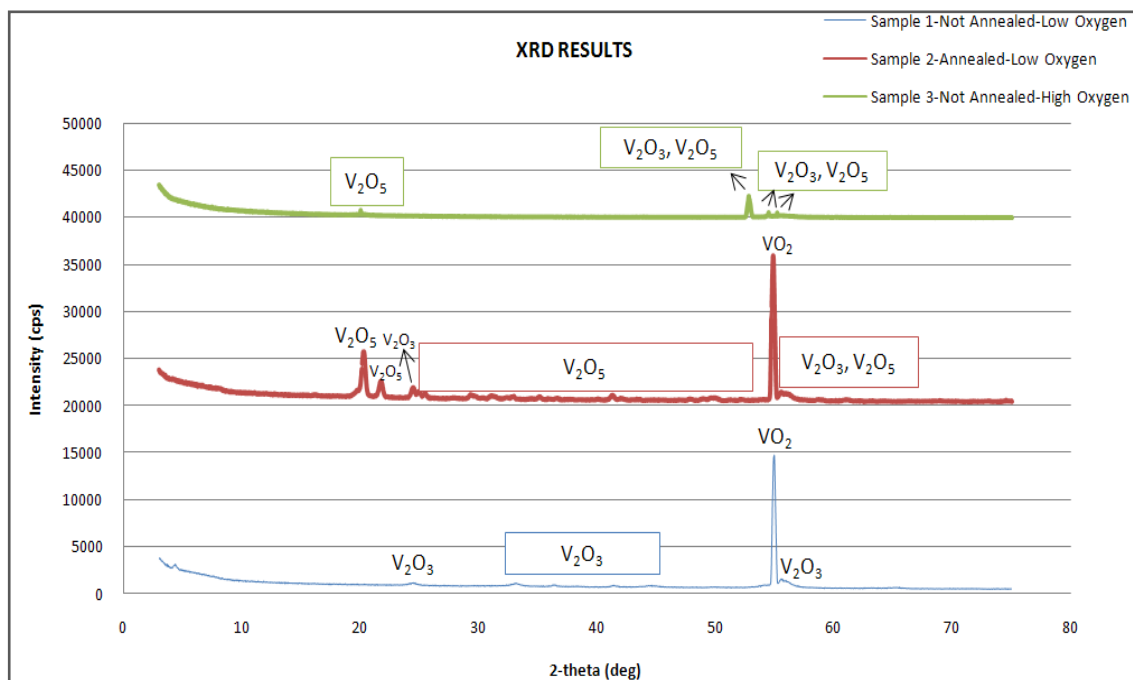


Figure 4.1: XRD results of the samples processed in different conditions. In Sample 1, the  $V_2O_3$  phase is dominant. After annealing, in the Sample 2,  $V_2O_5$  phase starts to be dominant. In sample 3, both  $V_2O_5$  and  $V_2O_3$  phases are observed.

While the Sample 1 contains  $V_2O_3$  phase mostly, after annealing of the sample, it shows the  $V_2O_5$  phase in its form. The same thing happens in the sample of which oxygen amount is increased during the deposition. These results support the information about  $VO_x$  phase transformation given in the literature [19].

In the low oxygen doped samples, Sample 1 and Sample 2,  $VO_2$  phase is also observed.  $VO_2$  is an intermediate form between the  $V_2O_3$  and  $V_2O_5$ . Figure 4.1 shows that after 1 hour annealing duration,  $V_2O_3$  is not completely transformed into  $V_2O_5$  phase. In the high oxygen doped sample, Sample 3, both  $V_2O_3$  and  $V_2O_5$  forms are observed. However, in this sample, the intermediate phase,  $VO_2$ , is not observed.

By the help of the XRD results, it is cleared that annealing or oxygen doping increase the  $V_2O_5$  phase in the  $VO_x$  samples. The XPS measurements of the samples given in Table 4.1 are also done. Table 4.2 shows both the  $V2p^3$  and  $V2p^1$  peak energies of the vanadium oxide samples and the comparison of these energies with the literature. The results observed with XPS do not show the same phases with the results observed with



XRD, since the measurement depth of the XPS is lower than the measurement depth of the XRD system. In XPS measurements, while only the surface of the samples is examined, in XRD measurements, the deeper thicknesses are analyzed.

Table 4.2: Comparison of the core level binding energies of the samples.

Core Level	Binding Energies (eV)					
	XPS Results in the Literature			XPS Results in This Study		
	G. A. Sawatzky and D. Post [27] University of Groningen			Sample 1	Sample 2	Sample 3
	V <sub>2</sub> O <sub>5</sub>	VO <sub>2</sub>	V <sub>2</sub> O <sub>3</sub>			
V2p <sup>3</sup>	516.9	516.2	515.7	515	515.5	515.5
V2p <sup>1</sup>	524.3	523.5	523.3	522.5	523.5	523

As it is seen from the table, while in the Sample 1, binding energies of the V2P<sup>3</sup> and V2P<sup>1</sup> peaks are lower; after annealing (in Sample 2) or after more oxygen doping (in Sample 3), the binding energies of the core levels shift to the higher levels.

Table 4.2 also states that the surfaces of the samples are not in the phase of VO<sub>2</sub> or V<sub>2</sub>O<sub>5</sub> phases yet. The binding energies of the core levels of Sample 2 and 3 are close to the binding energies of the V<sub>2</sub>O<sub>3</sub> given in the literature. However, in the surface of the Sample 1, the V2p<sup>3</sup> the peaks seem to be much lower than the peaks that V<sub>2</sub>O<sub>3</sub> phase takes, but it is away from being vanadium metal, the binding energy of vanadium metal peak is observed at 513.7 eV [28].

Since the XPS examines the surface of the sample, the phases found do not identify the characteristic of the whole sample. In the literature, there are some studies that show the change of the phases due to the depth of the vanadium oxide samples [19]. The material characteristic might be understood after examining the samples from the deeper points and different depths. In this study, since it examines the deeper points of the material, XRD measurements give enough information about the material characteristic.

## 4.2 Test Results

This section gives some of the TCR and noise measurement results of the vanadium oxide samples. The annealing and oxygen doping effects in the vanadium oxide deposition are tested in the TCR measurements.

### 4.2.1 TCR Measurements

In the literature, studies done on the  $VO_x$  thin films and resistors state that increasing resistivity also increases TCR of  $VO_x$  [19]. The reason is same with the resistivity rise, which is phase transformation. Resistivity increases increasing  $V_2O_5$  phase. Since  $V_2O_5$  has a high TCR property, increasing this phase also increases the TCR values. However, this is not the only way to find the high TCR values in the  $VO_x$  resistors,  $VO_2$  phases also show high TCR values as mentioned in Chapter 1. However achieving  $VO_2$  in the forms by sputtering method is more difficult than achieving  $V_2O_5$  [19].

The previous sections examine the effects of the annealing and the oxygen doping in the vanadium oxide depositions, while this section gives TCR changes of the annealed resistors. Since there is a problem on the etching of the high oxygen doped resistors (the uncontrolled etching of the vanadium oxide layer by the photoresist developer), the effect of the high oxygen doping to the resistors cannot be tested.

The samples for TCR measurements are chosen from the “not annealed-low oxygen doped” group, the resistances of the samples are increased by annealing method. TCR measurements of the resistors are done before and after the annealing process. The annealing of the samples are done on the hot plate. Table 4.3 shows the annealing process of the resistors, the change of the resistances and the TCR measurements.

Table 4.3: Resistance and TCR variations of the resistors before and after annealing step.

Resistor Sample	Annealing Duration (min)	Annealing Temperature (°C)	Initial Resistance @ 25°C	Initial TCR	Resistance After Annealing @ 25°C	Final TCR
2	15'	50	~2.3kΩ	0.74%/K <sup>-1</sup>	~142k	-1.6%/K <sup>-1</sup>
3	15'	50	~2.2kΩ	0.8%/K <sup>-1</sup>	~390k	-4.35%/K <sup>-1</sup>

Figure 4.2 and Figure 4.3 show the change of the resistances with temperature for Sample 2 and 3 before annealing the samples at 50 °C. Figure 4.4 and Figure 4.5 show the change of the resistances with temperature for Sample 2 and 3 after annealing the samples at 50°C. TCR values are calculated by the Formula 1.3 given in Chapter 1, which is given as  $\alpha = \frac{1}{R} \frac{dR}{dT} \cdot \frac{dR}{dT}$  is found from the slope of the resistance-temperature change graphs. R is the resistance value measured at 25 °C. The derivative of the equation shown on the graph gives the slope of the graph. The measurement results show that low resistance values have also low TCR values. After increasing the resistances by annealing process, both the resistance and TCR values are increased. The increase of the TCR of Sample 3 is much more than the increase of the TCR of Sample 2. As it is seen from the table, after annealing process, the resistivity value of Sample 3 is also higher than the resistivity value of the Sample 2.

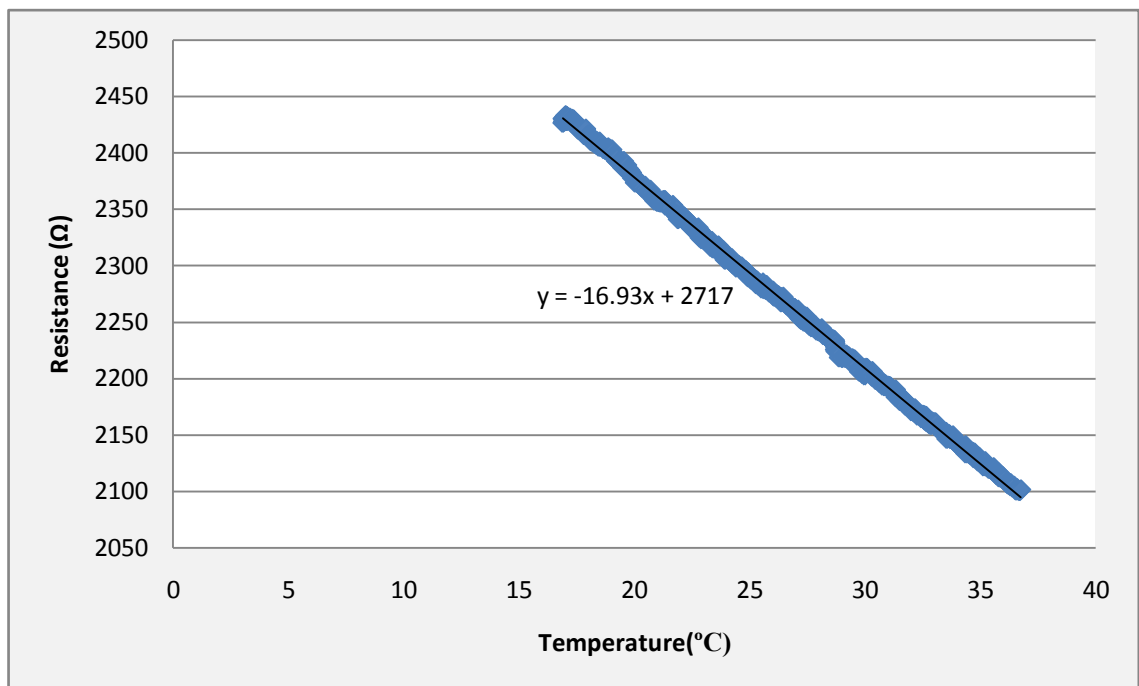


Figure 4.2: Resistance change with temperature, before annealing of Sample 2. The TCR of the resistor is calculated as -0.74%/K.

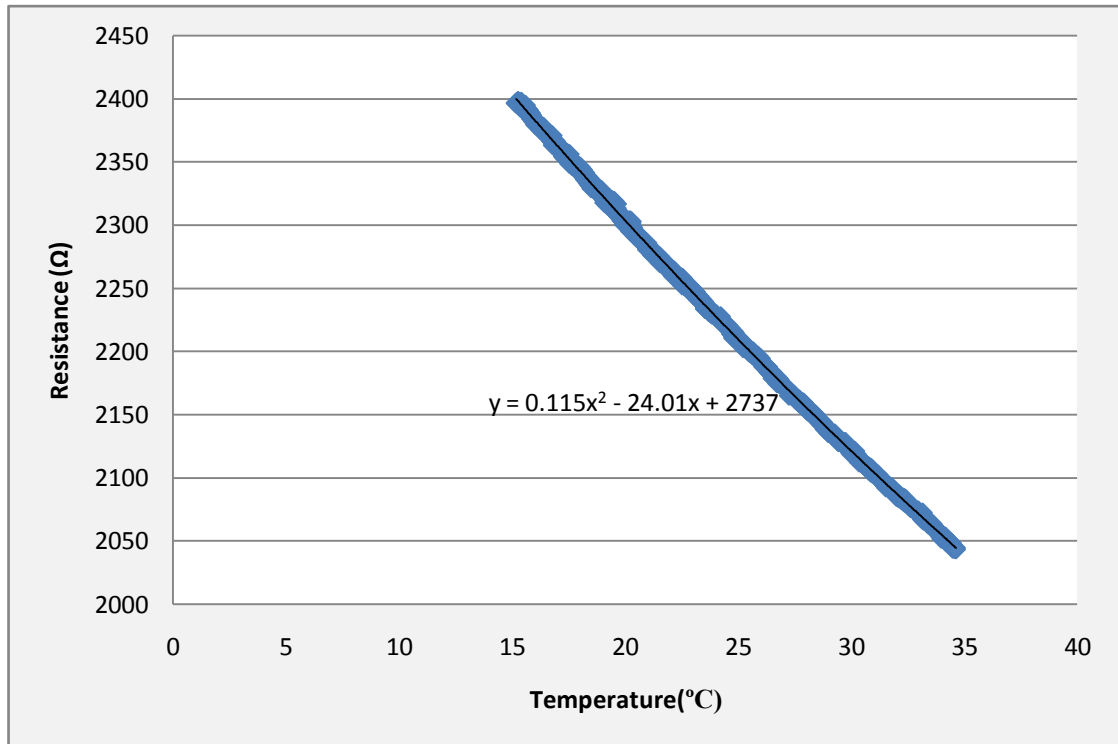


Figure 4.3: Resistance change with temperature, before annealing of Sample 3. The TCR of the resistor is calculated as 0.8 %/K.

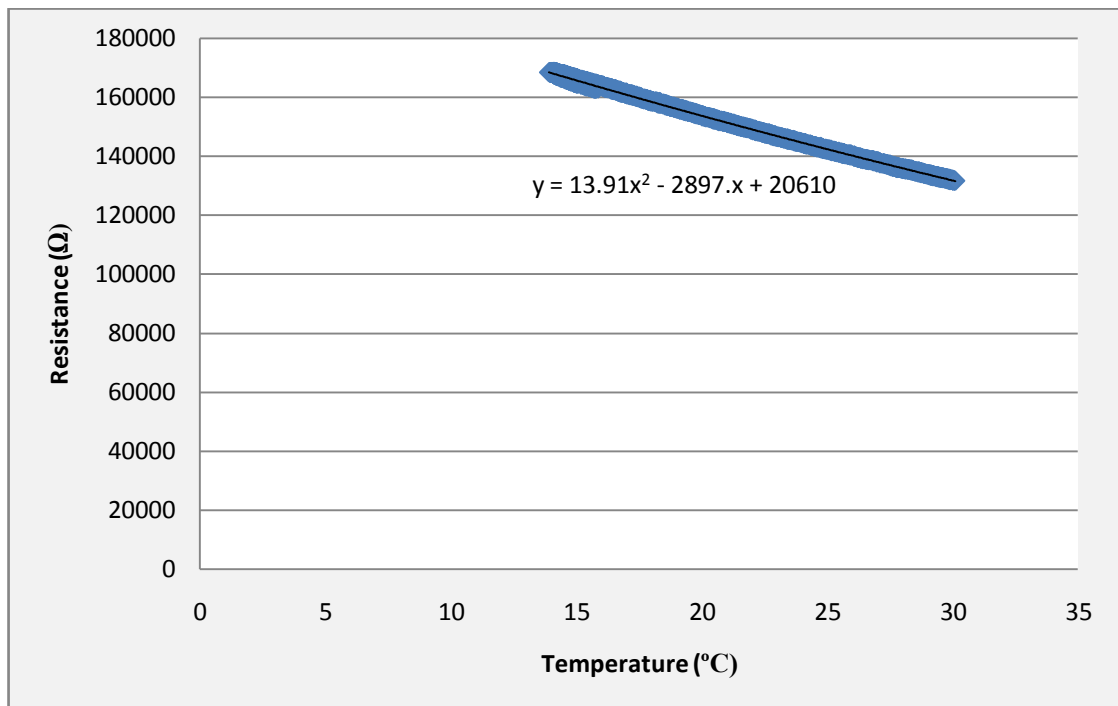


Figure 4.4: Resistance change with temperature, after annealing step of Sample 2. The TCR of the resistor is calculated as -1.6%/K.

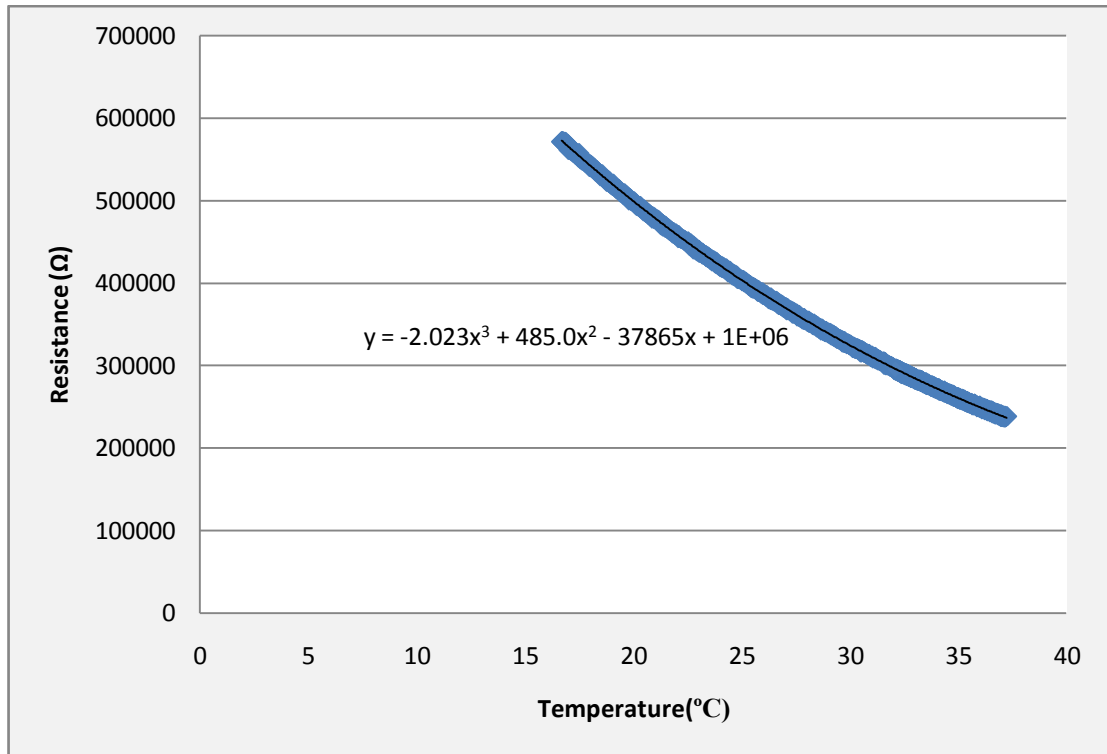


Figure 4.5: Resistance change with temperature, after annealing step of Sample 3. The TCR of the resistor is calculated as  $-4.35\%/K$ .

In the literature, in some studies, it is claimed that low resistive  $VO_x$  can show high TCR values [29]. However, in this study, this disquisition could not be verified.

#### 4.2.2 Noise Measurements

Noise of the detector is one of the key parameters for the performance of the microbolometer detectors. The noise of the resistor structure has two major components: thermal noise and  $1/f$  noise.

Under bias or no-bias conditions, every resistance has a thermal noise, but  $1/f$  noise appears only if there is a current on the resistor. The fabricated resistors are tested using a Charge Trans-impedance Amplifier (CTIA) followed by a voltage amplifier, all of which are placed inside nested Faraday Cages and an Agilent Dynamic Signal Analyzer. Figure 4.6 shows the simplified schematic of the circuit used for noise measurement of both resistors. This set-up is also used for the detector noise measurements.

During the noise measurements, two resistors with similar resistances are used since this will be the case within the actual imaging array. Therefore, it should be noted that the measured noise is due to both resistors. There is also a proper resistance value for this setup. The biasing circuitry in the readout of the microbolometer arrays that are designed in METU includes two transistors and two resistors, with a total voltage headroom of 5V. In case of very high detector resistance, the detector current would be very low due to limited voltage headroom.

If the resistances are too low, the bias current is increased and due to the self heating affect [6] the noise of the resistors start to increase.

On the other hand, in case of very low detector resistance, the current noise of the detector becomes very large. Although it is possible to increase the SNR of the output current by increasing the bias on the detector, the self heating effect limits the maximum allowable current and hence, the SNR.

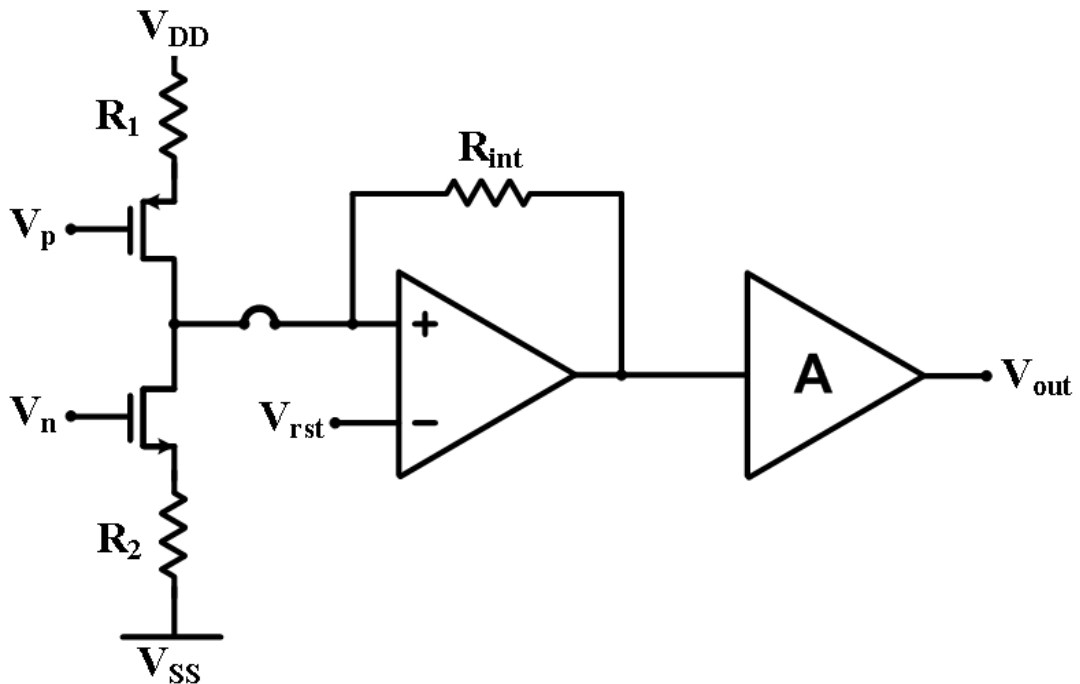


Figure 4.6: Simplified schematic of the noise measurement setup used in the measurements.

The aforementioned limitations in the readout due to the resistance values obstruct the measurements. Therefore annealed resistors are used in these measurements either. Figure 4.7 and Figure 4.8 show the noise measurement results of the samples. The recipes of the samples are same with the ones used in the TCR measurements and are listed in Table 4.4. However, as it is seen from the figure, the final resistances after annealing step are not same with the ones with the final resistance values observed in the samples with the same recipes given in Chapter 3.

Table 4.4: The recipes of the samples which are prepared for the noise measurements.

Resistor Sample	Annealing	Annealing Duration (min)	Annealing Temperature (°C)	Initial Resistance @ 25°C	Final Resistance After Annealing @ 25°C
2	on hotplate	15'	50	~2.3kΩ	~115k
3	on hotplate	15'	50	~2.2kΩ	~85k

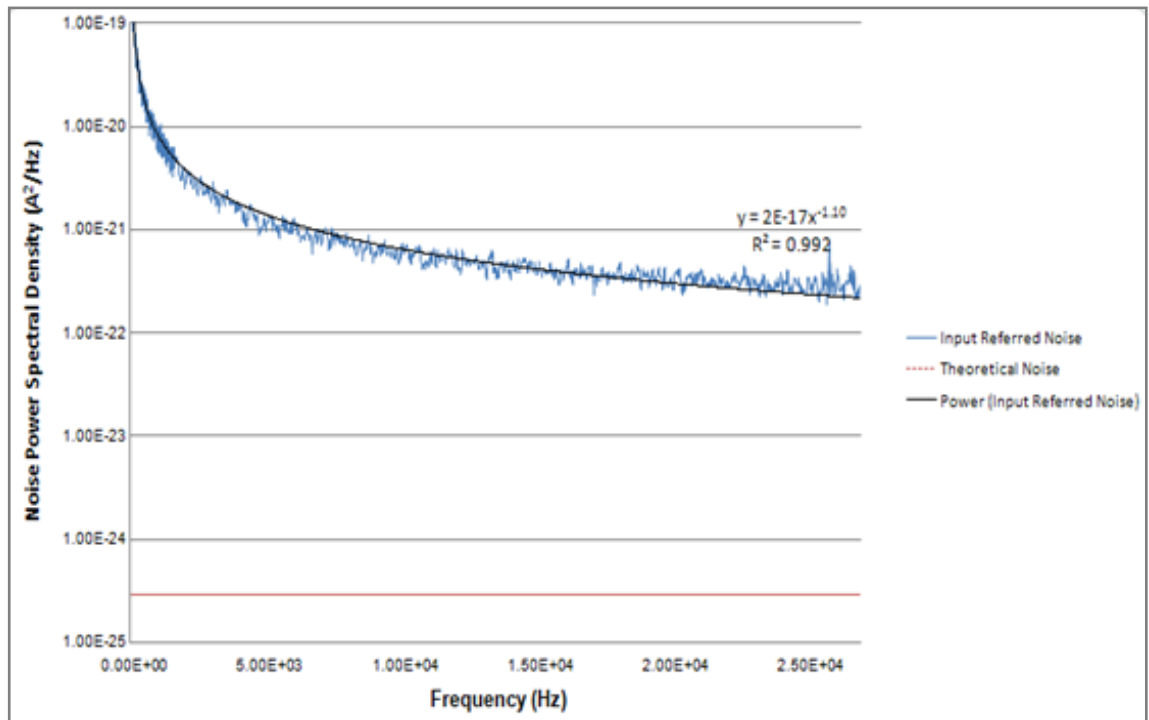


Figure 4.7: The noise measurement result of the 115k resistor. The corner frequency is ~3.28 MHz.<sup>(3)</sup>

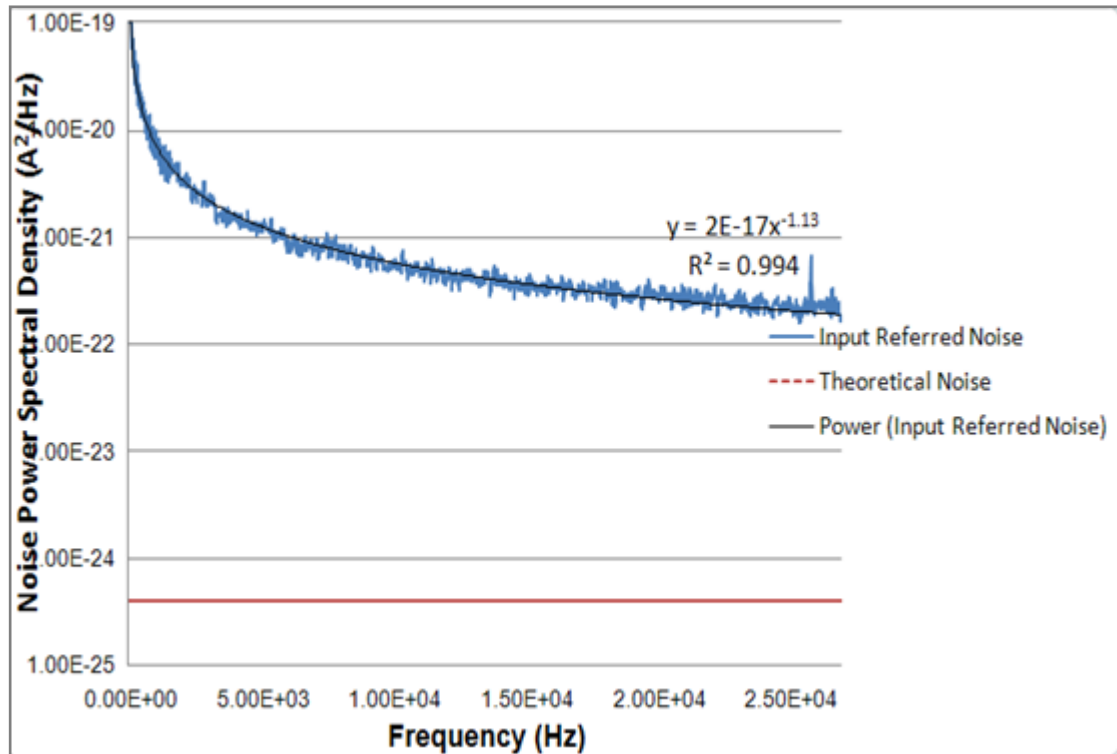


Figure 4.8: The noise measurement result of the 85k resistor. The corner frequency is 2.63MHz.<sup>(3)</sup>

The corner frequencies of the 85k and 115k resistors are 2.63 and 3.276 MHz, respectively. These values are too high for the VO<sub>x</sub> resistors. Figure 4.9 shows the previous noise test result taken from the YBCO resistors.

As it is seen from the figure, the corner frequency of these YBCO resistors are far less than the values found for the VO<sub>x</sub> resistors, however, there are numerous studies found in the literature in which noise of the VO<sub>x</sub> resistors are lower than the YBCO resistors. The main reason to use VO<sub>x</sub> as an active material layer is the lower noise as it is previously discussed.

The reason of this significantly high noise is probably due to the residual VO<sub>x</sub> on the electrodes. This contamination prevents an accurate measurement.

<sup>3</sup> The noise measurements are done by Miss Şeniz Esra Küçük.



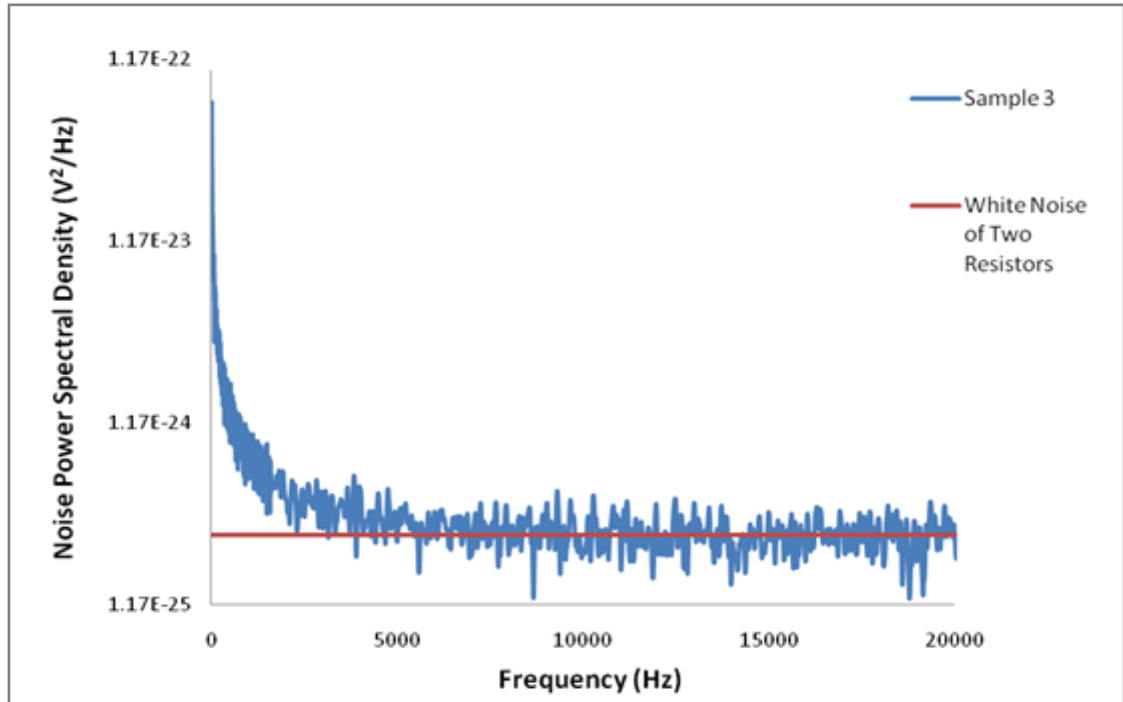


Figure 4.9: A noise test result of the YBCO resistor, previously measured for the YBCO resistor optimizations [20].

### 4.3 Conclusions

The XRD results show that  $V_2O_5$  phase transition occurs after annealing the “low oxygen doped-not annealed” sample. The same thing is observed by increasing the oxygen ratio in the low oxygen doped-not annealed sample. This means that annealing or increasing oxygen amount avails to have high TCR vanadium oxide.

The TCR results of the samples are increased by annealing the resistors as it is expected. Moreover, the resistances after the annealing of the sample resistors prepared for TCR measurements are not similar with the resistance values of the resistors which are prepared with the same recipe and given in Chapter 3. These results show the unreliability of the annealing on the hot plate.

Moreover, in the noise measurement results, the corner frequencies calculated are over the expected corner frequencies. However, compared with the YBCO resistors, the noise of the  $VO_x$  resistors should be much lower. The contamination on the surface of the electrodes is the probable reason of these unexpected values.

# CHAPTER 5

## CONCLUSION

This thesis reports the development and optimization of vanadium oxide ( $\text{VO}_x$ ) material for microbolometer detectors. Magnetron sputtering technique is used to develop  $\text{VO}_x$  as a high performance detector active material. Optimum deposition conditions of magnetron sputtering system are investigated to make  $\text{VO}_x$  resistors. In these resistors, high TCR, compatibility with the literature, and proper resistance values (50-100 k $\Omega$  resistances) with the microbolometer detector readout are aimed. Since,  $\text{VO}_x$  resistors are fabricated, for the first time in METU, identification of the material is done firstly.

The achievements gained during this research can be summarized and listed as follows:

- A vanadium target is used to develop vanadium oxide; thickness and resistivity uniformity optimizations of vanadium target are done. Effects of different deposition parameters of the magnetron sputtering system on the vanadium oxide depositions are investigated. The influence of the change of the parameters on the resistivity and thickness values of  $\text{VO}_x$  are examined in detail. Briefly, resistivity of the thin film vanadium oxide decreases while the dc power increases; on the contrary, the resistivity of  $\text{VO}_x$  increases when the substrate temperature, annealing temperature or annealing duration, and oxygen ratio of the deposition increase. Comparison of the optimization results with the literature is done, and it is observed that very compatible results with the studies done on  $\text{VO}_x$  in the literature are obtained.
- Optimum resistor type and optimum electrode type are chosen among the various resistor and electrode types for the  $\text{VO}_x$  resistors. Planar resistors are used to make the optimizations of  $\text{VO}_x$ . Considering the proper (50-100 k $\Omega$  resistances) resistor values convenient with the readout of the microbolometer detectors, also by taking into account the resistor and electrode type chosen; the most convenient deposition recipe of vanadium oxide is determined.

- Process modifications of the planar resistors are carried out; finger electrodes' metal RIE optimizations are done. Platinum target optimizations are tackled. Etching trials of platinum thin films are carried out to use platinum in the electrodes rather than gold in the future studies.
- Etching of the low resistive vanadium oxide films is optimized. The effects of the deposition parameters on the vanadium oxide etching are identified. The reason of the etching problem is stated as the change of the phases formed in the developed mixed phase vanadium oxide. It is also considered that annealing and oxygen amount parameters in the VO<sub>x</sub> deposition are the dominant factors to change the vanadium oxide material characteristic. Impact of the annealing and oxygen amount parameters on the etching of the VO<sub>x</sub> films are researched inclusively.
- Fabrication of the low ( $9 \times 10^{-4} \Omega \cdot \text{cm}$ ) and high (250  $\Omega \cdot \text{cm}$ ) resistive VO<sub>x</sub> resistors using magnetron sputtering system are done successfully. Resistance measurements of the resistors are done and it is observed that increasing annealing or oxygen amount during the deposition of VO<sub>x</sub>, increases the resistance values of the resistors or vice versa.
- To make the resistors' resistances compatible with the resistances necessary for the CMOS applications, literature search is done to rise or to reduce the resistances of VO<sub>x</sub> resistors, the methods which are convenient with the facilities in METU are identified. These methods are tried on the resistors with low and high resistance values. Annealing the resistors on the hot plate is used to increase the resistances. In the resistor measurements, it is observed that increasing annealing duration increases the resistor values.
- The problems encountered during the processes are stated. New experiments are done to solve the contamination on the electrode, and the etching of VO<sub>x</sub> by the photoresist developer. A new process flow is created and tried out to solve both of these problems, but it needs more optimizations.
- Sample resistors for the TCR measurements are prepared by annealing method, on the hot plate. The TCR measurements of these resistors are done. It is observed that, increasing resistance on the resistors increases the TCR values. These are the expected values compared with the literature. Sample resistors for the noise measurements are prepared by annealing method, as in TCR measurements.

In this study, an overall idea about the vanadium oxide films; about their resistivity and sheet resistance values are achieved, there are many studies should be done to develop a high performance resistor.

- The contamination problem seen on the electrodes should be solved. A new process flow can solve the problems encountered. In this process flow, the electrodes will be on the active material layer to prevent the contamination, and nitride layer can be coated on the resistors to prevent the etching of the photoresist developer. Since the high noise values measured, the “contamination” can be called as the main problem. A new process flow is designed to get rid of this problem, but it has not been applied yet. The new process flow is provided in Appendix, and it can be used in the future, since the vanadium oxide layer is coated on the electrodes, the etching of the gold layer will not be a problem.
- Platinum electrodes will be studied further. The Metal RIE etching of the platinum electrodes should be finished.

As a conclusion, this thesis reports the optimizations of the vanadium oxide thin film as an active infrared detector material by magnetron sputtering method. The most proper deposition recipe for the CMOS applications is determined. However, in the course of the resistor fabrications, it is understood that the resistors cannot be fabricated by using this recipe because of the uncontrollable etching of the vanadium oxide layer by the photoresist developer. The problem occurred during the fabrication process is not only this unexpected etching, but also the contamination occurs on the electrodes is another major problem. It is observed that this contamination makes the resistances of the resistors unreliable. This unreliability of the resistances is observed both on the TCR and the noise measurements. Trials are done to get rid of this problem but a permanent solution could not have been found. On the other hand, the Metal RIE etching of the electrodes are also studied and developed. A new material, platinum is started to be optimized to be used in the electrodes. In addition, the characterizations of the vanadium oxide films are done and the relation between the deposition conditions of the vanadium oxide and the characteristic of the material is identified. In the future work, the problems encountered will be obstructed by the new process flow designed provided in Appendix.

## REFERENCES

[1] [http://www.practicalphysics.org/go/Resources\\_16.html](http://www.practicalphysics.org/go/Resources_16.html), last accessed on 08.02.2011

[2] A. D. Dave, “Micromachined Infrared Sensors with Device-Level Encapsulation,” Dissertation for the Degree of Master of Science, University of Texas at Arlington, Department of Electrical Engineering, May 2005.

[3] E. L. Dereniak and G. D. Boreman, *Infrared Detectors and Systems*, John Wiley & Sons Inc., Academic Press, 1996.

[4] <http://www.theses.ulaval.ca/2005/23016/apb.html>, last accessed on 08.02.2011.

[5] <http://www.newport.com/Laws-of-Radiation/381843/1033/catalog.aspx>, 08.02.2011

[6] M. Y. Tanrikulu, “An Uncooled Infrared Microbolometer Array Using Surface Micromachined MEMS Technology,” *Dissertation for the Degree of Doctor of Philosophy*, METU, in Department of Electrical and Electronics Engineering, 2007.

[7] Jun Dai et al., “Low Temperature Fabrication Of  $\text{VO}_x$  Thin Films For Uncooled IR Detectors By Direct Current Reactive Magnetron Sputtering Method,” *Infrared Physics & Technology*, Vol. 51, pp. 287–291, 2008.

[8] F. Civitci, “Development of High Fill Factor Uncooled Infrared Detector Pixels,” *Dissertation for the Degree of Master of Science*, METU, in Department of Electrical and Electronics Engineering, 2008.

[9] U. Senveli, “Development of High Thermal Performance Uncooled Infrared Detector Pixels With Enhanced Resistor Structures”, *Dissertation for the Degree of Master of Science*, METU, 2010.

[10] T. B. Watkins, “1/F Noise In Germanium Devices,” *Surrey Proc. Phys. Soc.*, pp. 73:59, 1959.

[11] M. A. Todd, P. P. Donohue, R. Watton, C. J. Anthony, “High-Performance Ferroelectric and Magnetoresistive Materials for Next-Generation Thermal Detector Arrays,” *Proc. SPIE, Hot and Uncooled IR Detector Materials*, Vol 4795, pp. 88-99, 2002.

[12] B. Wang, S.B. Zhou, G. Huang, B.F. Xiong, S.H. Chen, X.J. Yi, “Fabrication of 128-128 Element Optical Switch Array by Micromachining Technology,” *Microprocessors and Microsystems*, vol. 29, pp. 21–25, 2004.

- [13] S. Chen, H. Ma, S. Wang, N. Shen, J. Xiao, and X. Zhao, "Vanadium Oxide Thin Films Deposited on Silicon Dioxide Buffer Layers by Magnetron Sputtering," *Thin Solid Films*, vol. 497, pp. 267 – 269, 2006.
- [14] S. Chen, H. Ma, S. Xiang, and X. Yi, "Fabrication And Performance of Microbolometer Arrays Based on Nanostructured Vanadium Oxide Thin Films," *Smart Materials and Structures*, pp. 696–700, 2007.
- [15] N. Fieldhouse, M Purse, M. W Horn "Electrical Properties of Vanadium Oxide Thin Films for Bolometer Applications: Processed by Pulse Dc Sputtering," *J. Phys. D: Appl. Phys.*, pp. 42-6, 2009.
- [16] K. G. West, J. Lu, J. Yu, D. Kirkwood, W. Chen, Y. Pei, J. Claassen, S. A. Wolf, "Growth and Characterization of Vanadium Dioxide Thin Films Prepared by Reactive-Biased Target Ion Beam Deposition," *J. Vac. Sci. Technol.*, pp. 26-133, 2008.
- [17] Y. S. Yoon, J. S. Kim and S. H. Choi, "Structural And Electrochemical Properties Of Vanadium Oxide Thin Films Grown By D.C. and R.F. Reactive Sputtering At Room Temperature," *Thin Solid Films*, Vol. 460, pp. 41-47, 2004.
- [18] <http://library.bldrdoc.gov/docs/nbshb100.pdf> . last accessed on 08.02.2011
- [19] M. G. Krishna, Y. Debaugue and A. K. Bhattacharya, "X-Ray Photoelectron Spectroscopy and Spectral Transmittance Study of Stoichiometry in Sputtered Vanadium Oxide Films", *Thin Solid Films*, Vol. 312, pp. 116-122, 1998.
- [20] E. Canga, "Development and Characterization of High TCR Material for Surface Micromachined Microbolometers," *Dissertation for the Degree of Master of Science*, METU, in Department of Physics. M.Sc. Thesis, 2008.
- [21] <http://www.biology-online.org/articles/aqua-regia.html> Last Accessed on 08.02.2011
- [22] George F. Vander Voort, "Metallography, Principles and Practice," *Technology & Engineering*, pp.247, 1999.
- [23] A. Cheremisin, V. Putrolaynen, A. Velichko, A. Pergament, N. Kuldin, and A. Grishin, "UV Laser Modification And Selective Ion-Beam Etching Of Amorphous Vanadium Pentoxide Thin Films," *Physica Status Solidi*, Vol. 206, pp. 1484-1487, 2009.
- [24] H. Gin Nam, M. Shin, N. Cho, E. Yun, "Feasibility of Using Vanadium to Form Damascene Structures with an Air Gap," *Current Applied Physics*, pp. 667-670, 2007.
- [25] J. Li, N. Yuan, J. Xie, "Annealing Characteristics of The Vanadium Oxide Films Prepared by Modified Ion Beam Enhanced Deposition," *Applied Surface Science*, Vol. 243, pp. 437-442, 2005.

- [26] Y. Lv, M. Hu, M. Wu, Z. Liu, "Preparation of Vanadium Oxide Thin Films With High Temperature Coefficient of Resistance by Facing Targets D.C. Reactive Sputtering and Annealing Process," *Surface and Coatings Technology*, Vol. 201, pp. 4969-4972, 2007.
- [27] G. A. Sawatzky and D. Post, "X-Ray Photoelectron and Auger Spectroscopy Study of Some Vanadium Oxides," *Phys. Rev.*, B 20, pp. 1546–1555, 1979.
- [28] N. Alov, D. Kutsko, I. Spirovová, and Z. Bastl, "XPS Study Of Vanadium Surface Oxidation by Oxygen Ion Bombardment," *Surface Science*, Vol. 600, pp. 1628-1631, 2006.
- [29] C. Venkatasubramanian, M. W. Horn, and S. Ashok, "Ion Implantation Studies On  $\text{Vo}_x$  Films Prepared By Pulsed Dc Reactive Sputtering", *Nuclear Instruments and Methods in Physics Research* , Vol. 267, pp. 1476-1479, May 2009.

## APPENDIX A

### NEW PROCESS FLOW DESIGNED FOR THE VO<sub>x</sub> RESISTORS

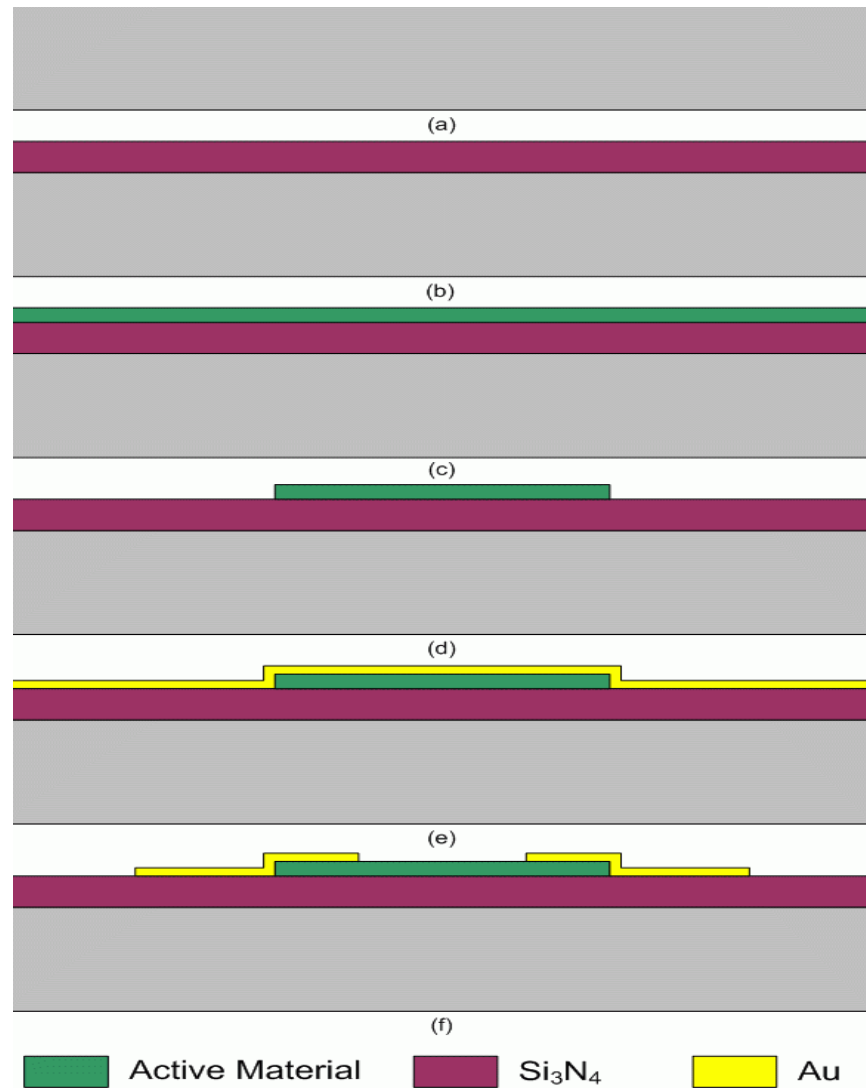


Figure A.1: New process flow designed to prevent the contamination on the electrodes. (a) A silicon wafer is taken, (b) nitride layer is coated on the silicon wafer as isolation, (c) active material layer is coated, and (d) patterned, (e) electrode layer is deposited on the vanadium oxide, and (f) electrode layer is patterned.